Accurate Mass Determination in SUSY-like Events with Missing Energy

Jack Gunion
U.C. Davis

Fermilab, March 6, 2008

Collaborators: Hsin-Chia Cheng, Dalit Engelhardt, Zhenyu Han, Guido Marandella, Bob McElrath

Based on arXiv:0707.0030 and arXiv:0802.4290.

Motivations for an invisible particle below the TeV Scale

1. To solve the Higgs boson mass hierarchy problem there must be new particles below the TeV scale.

2. Sub-TeV new physics avoids precision electroweak constraints most easily if there is a new discrete symmetry that requires that they couple in pairs to the SM particles (especially, the W and Z).

3. The lightest such new particle will then be stable and could explain the observed dark matter in the universe.

4. In many models the correct dark matter density can be obtained and it will have evaded observational contraints (dark matter detection, ...) if this new particle is weakly interacting, $\rightarrow$ WIMP

   $\Rightarrow$ $\mathbf{2}$ such particles (call them N) per LHC event that lead to variable and partially balancing missing momentum in each event.

Popular Candidate Models

- **SUSY with R-parity conservation.**

  The lightest supersymmetric particle (LSP) is likely to be a neutralino, which is a good WIMP candidate.

- **Little Higgs Models with T-parity: lightest T-odd particle is a good WIMP.**

- **Universal Extra Dimensions: lightest KK mode (e.g. first excited 'photon') is a good WIMP.**

- **Models with warped unification with Z_3 parity, ...**

Given the probable ILC time scales, the big question is if the LHC alone will be able to measure the properties of the WIMP candidate *with the accuracy needed to check that its predicted relic density is consistent with observation*.

A very crucial part of the answer involves the accuracy with which mass scales can be determined at the LHC in the presence of missing energy!

The problem: For all except really lengthy decay chains, if there is a pair of invisible particles, then there is not enough information to reconstruct the kinematics of each event *on an event-by-event basis*.

- **Mass scales will be important not only for the dark matter issue but also for the LHC inverse problem: Can we use LHC data to determine the fundamental Lagrangian parameters?**
  And, can we do so with sufficient accuracy as to allow a meaningful extrapolation to the GUT scale?
  The general picture:

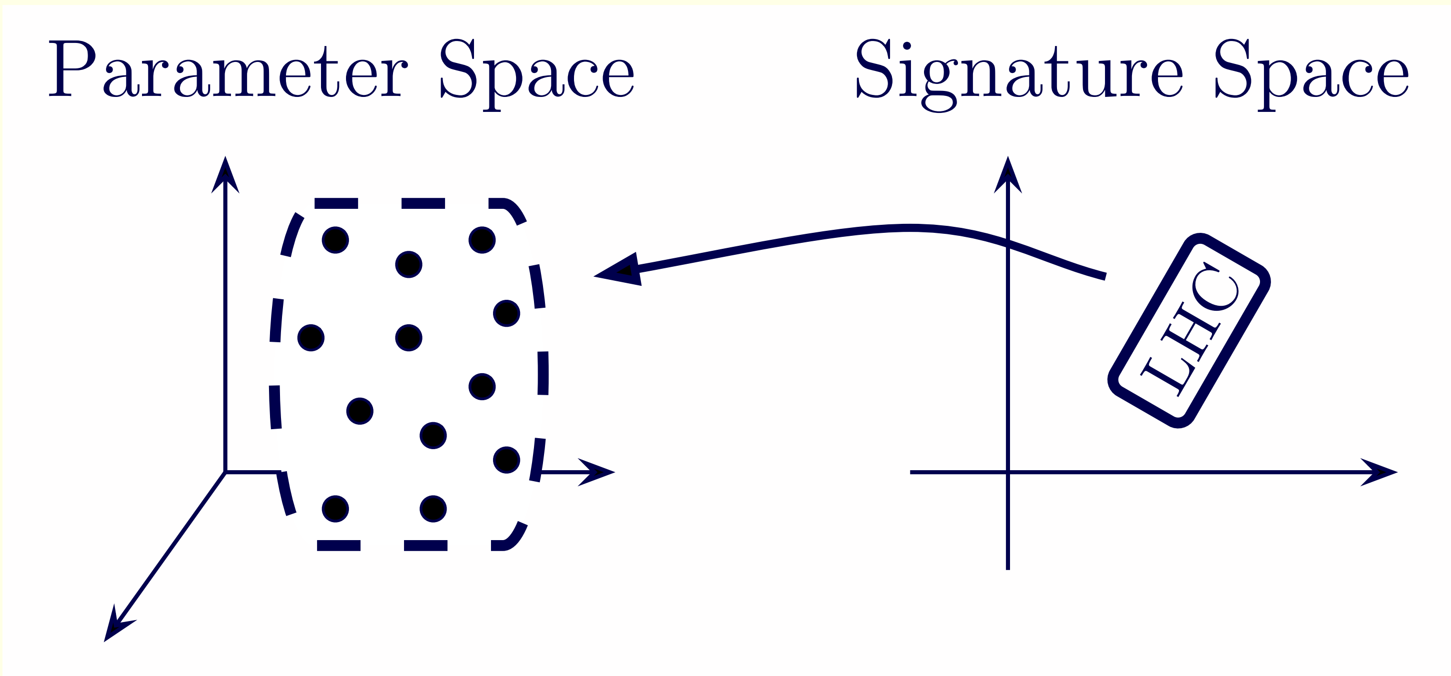

Figure 1: *The likely LHC situation. N. Arkani-Hamed, G. L. Kane, J. Thaler and L. T. Wang, JHEP* **0608***, 070 (2006) [arXiv:hep-ph/0512190].*

The picture is particularly bad if the LHC will have a hard time determining the absolute mass scale.

As an example of the difficulties encountered, let us consider the mSUGRA SPS1a point with GUT-scale parameters

$$m_0 = 100 \text{ GeV}, m_{1/2} = 250 \text{ GeV}, A_0 = -100 \text{ GeV}, \tan\beta = 10, \mu > 0 \,. \tag{1}$$

The decay chain of interest will be

$$\widetilde{q}_L \to q\,\widetilde{\chi}^0_2 \to q\,\ell\,\widetilde{\ell}_R \to q\,\ell\,\overline{\ell}\,\widetilde{\chi}^0_1, \quad (\ell = e, \mu), \tag{2}$$

with the relevant masses being (some variation with program)

$$m_{\widetilde{\chi}^0_1}, m_{\widetilde{\ell}_R}, m_{\widetilde{\chi}^0_2}, m_{\widetilde{u}_L/\widetilde{d}_L} = 97.4, 142.5, 180.3, 564.8/570.8 \text{ GeV} \,. \tag{3}$$

Using lepton spectrum edges and the like, one gets a good determination of mass differences, but a really precise determination of the overall mass scale is elusive — $m_{\widetilde{\chi}^0_1}$ sets the overall scale.

ATLAS studied mass determination using edges. The early results summarized in the LHC/LC project (hep-ph/0403133 with $L = 300 \text{ fb}^{-1}$) are:

$$\Delta m_{\widetilde{\chi}^0_1} \sim \Delta m_{\widetilde{\chi}^0_2} \sim \Delta m_{\widetilde{\ell}_R} \sim 4.8 - 5 \text{ GeV},$$
$$\Delta m_{\widetilde{q}_L} \sim 9 \text{ GeV} \,, \quad \Delta m_{\widetilde{g}} \sim 8 \text{ GeV}.$$

For SPS1a, the LHC cannot determine $m_{\widetilde{\chi}_1^\pm}$ and $m_{\widetilde{\nu}_{e,u,\tau}}$ accurately.

ILC data (assuming $\sqrt{s} \leq 1~\mathrm{TeV}$) from a series of threshold scans yields accuracies of

$$\Delta m_{\widetilde{\chi}_1^0} \sim \Delta m_{\widetilde{e}_R} \sim 0.05~\mathrm{GeV}, \quad \Delta m_{\widetilde{\mu}_R} \sim 0.2~\mathrm{GeV}\,, \quad \Delta m_{\widetilde{\chi}_2^0} \sim 1.2~\mathrm{GeV}\,,$$
$$\Delta m_{\widetilde{\chi}_1^\pm} \sim 0.5~\mathrm{GeV}\,, \quad \Delta m_{\widetilde{\nu}_e} \sim 1.2~\mathrm{GeV}\,,$$
$$\Delta m_{\widetilde{q}_L} \sim N/A.\,, \quad \Delta m_{\widetilde{g}} \sim N/A$$

Combining LHC and ILC gives (because mass differences are so well known and the absolute mass scale is well determined by the ILC $m_{\widetilde{\chi}_1^0}$ measurement)

$$\Delta m_{\widetilde{\chi}_1^0} \sim \Delta m_{\widetilde{e}_R} \sim 0.05~\mathrm{GeV}\,, \quad \Delta m_{\widetilde{\mu}_R} \sim 0.2~\mathrm{GeV}\,, \quad \Delta m_{\widetilde{\chi}_2^0} \sim 0.08~\mathrm{GeV}\,,$$
$$\Delta m_{\widetilde{\chi}_1^\pm} \sim 0.5~\mathrm{GeV}\,, \quad \Delta m_{\widetilde{\nu}_e} \sim 1.2~\mathrm{GeV}\,,$$
$$\Delta m_{\widetilde{q}_L} \sim 5~\mathrm{GeV}\,, \quad \Delta m_{\widetilde{g}} \sim 6.5~\mathrm{GeV}$$

An updated study gives the results of Table 1. Note the presence of two possible minima (the two different peaks in the plot Meena showed).

	Nom	(1,1) $\langle m \rangle$	σ	γ_1	(1,2) $\langle m \rangle$	σ	γ_1
$m_{\tilde{\chi}_1^0}$	96.1	96.3	3.8	0.2	85.3	3.4	0.1
$m_{\tilde{l}_R}$	143.0	143.2	3.8	0.2	130.4	3.7	0.1
$m_{\tilde{\chi}_2^0}$	176.8	177.0	3.7	0.2	165.5	3.4	0.1
$m_{\tilde{q}_L}$	537.2	537.5	6.1	0.1	523.2	5.1	0.1
$m_{\tilde{b}_1}$	491.9	492.4	13.4	0.0	469.6	13.3	0.1
$m_{\tilde{l}_R} - m_{\tilde{\chi}_1^0}$	46.92	46.93	0.28	0.0	45.08	0.72	-0.2
$m_{\tilde{\chi}_2^0} - m_{\tilde{\chi}_1^0}$	80.77	80.77	0.18	0.0	80.18	0.29	-0.1
$m_{\tilde{q}_L} - m_{\tilde{\chi}_1^0}$	441.2	441.3	3.1	0.0	438.0	2.7	0.0
$m_{\tilde{b}_1} - m_{\tilde{\chi}_1^0}$	395.9	396.2	12.0	0.0	384.4	12.0	0.1

Table 1: SPS 1a (α): Minima for $\Delta\Sigma \leq 1$ in regions *(1,1)* and *(1,2)*. Ensemble means, $\langle m \rangle$, and root-mean-square distances from the mean, σ, are in GeV. The three lightest masses are very correlated. The mass of $\tilde{q}_L$ is fairly correlated to the lighter masses, but $m_{\tilde{b}_1}$ is essentially uncorrelated. The distributions are very close to symmetric.

How does the LHC accuracy compare to what is needed?

a) A precision calculation of the dark matter primarily needs accurate masses (couplings being fixed by supersymmetry). For SPS1a (bulk region), can get 10% accuracy for Ω_χ with 5% errors on masses (keeping couplings, ... fixed).

b) What is needed to meaningfully assess GUT scale boundary conditions? From hep-ph/0403133, for SPS1a and using the errors obtained combining LHC and ILC data as given above, they find GUT-scale errors of

$$\Delta M_1 = 0.15~\mathrm{GeV}, \Delta M_2 = 0.25~\mathrm{GeV}, \Delta M_3 = 2.3~\mathrm{GeV},$$
$$\Delta m_0(L_1) = 6~\mathrm{GeV}, \Delta m_0(Q_1) = 23~\mathrm{GeV}~.$$

Corresponding errors for LHC data alone for SPS1a are currently under debate. Sfitter (arXiv:0709.3985v2) claims in particular to get M_2, contrary to earlier LHC/LC study where $m_{\widetilde\chi_1^\pm}$ was hard to determine.

	LHC	ILC	LHC+ILC	SPS1a
$\tan\beta$	9.8 $\pm$ 2.3	17.6 $\pm$ 9.6	16.4 $\pm$ 7.0	10.0
M_1	101.5 $\pm$ 4.6	102.8 $\pm$ 0.72	102.7 $\pm$ 0.53	103.1
M_2	191.7 $\pm$ 4.8	192.3 $\pm$ 2.6	191.7 $\pm$ 1.7	192.9
M_3	575.7 $\pm$ 7.7	fixed 500	578.0 $\pm$ 6.3	577.9
$M_{\tilde{e}_L}$	192.7 $\pm$ 5.3	194.4 $\pm$ 0.24	194.4 $\pm$ 0.22	194.4
$M_{\tilde{e}_R}$	134.0 $\pm$ 4.8	135.8 $\pm$ 0.17	135.7 $\pm$ 0.12	135.8
$M_{\tilde{q}3_L}$	478.2 $\pm$ 9.4	509.1 $\pm\mathcal{O}(2\cdot 10^2)$	489.6 $\pm$ 10.7	480.8
$M_{\tilde{q}_L}$	523.6 $\pm$ 8.4	fixed 500	526.7 $\pm$ 4.9	526.6
$M_{\tilde{q}_R}$	506.2 $\pm$ 11.7	fixed 500	508.2 $\pm$ 10.8	508.1
A_t	-500.6 $\pm$ 58.4	-521.8 $\pm$ 160.1	-490.3 $\pm$ 166.8	-490.9
m_A	446.1 $\pm\mathcal{O}(10^3)$	393.4 $\pm$ 1.1	393.4 $\pm$ 1.1	394.9
μ	350.9 $\pm$ 7.3	355.2 $\pm$ 2.5	355.2 $\pm$ 2.3	353.7
m_t	171.4 $\pm$ 1.0	171.4 $\pm$ 0.12	171.4 $\pm$ 0.12	171.4

Table 2: Result for the general MSSM parameter determination in SPS1a assuming vanishing theory errors. As experimental measurements the kinematic endpoint measurements are used for the LHC column, and the mass measurements given for the ILC column. In the LHC+ILC column these two measurements sets are combined. Shown are the nominal parameter values and the result after fits to the different data sets. All masses are given in GeV.

	LHC	ILC	LHC+ILC	SPS1a
$\tan\beta$	10.0 $\pm$ 4.5	12.1 $\pm$ 7.0	12.6 $\pm$ 6.2	10.0
M_1	102.1 $\pm$ 7.8	103.3 $\pm$ 1.1	103.2 $\pm$ 0.95	103.1
M_2	193.3 $\pm$ 7.8	194.1 $\pm$ 3.3	193.3 $\pm$ 2.6	192.9
M_3	577.2 $\pm$ 14.5	fixed 500	581.0 $\pm$ 15.1	577.9
$M_{\tilde{\mu}_L}$	193.2 $\pm$ 8.8	194.5 $\pm$ 1.3	194.5 $\pm$ 1.2	194.4
$M_{\tilde{\mu}_R}$	135.0 $\pm$ 8.3	135.9 $\pm$ 0.87	136.0 $\pm$ 0.79	135.8
$M_{\tilde{e}_L}$	193.3 $\pm$ 8.8	194.4 $\pm$ 0.91	194.4 $\pm$ 0.84	194.4
$M_{\tilde{e}_R}$	135.0 $\pm$ 8.3	135.8 $\pm$ 0.82	135.9 $\pm$ 0.73	135.8
$M_{\tilde{q}3_L}$	481.4 $\pm$ 22.0	499.4 $\pm\mathcal{O}(10^2)$	493.1 $\pm$ 23.2	480.8
$M_{\tilde{q}_L}$	524.6 $\pm$ 14.5	fixed 500	526.1 $\pm$ 7.2	526.6
$M_{\tilde{q}_R}$	507.3 $\pm$ 17.5	fixed 500	509.0 $\pm$ 19.2	508.1
A_t	-509.1 $\pm$ 86.7	-524.1 $\pm\mathcal{O}(10^3)$	-493.1 $\pm$ 262.9	-490.9
m_A	406.3 $\pm\mathcal{O}(10^3)$	393.8 $\pm$ 1.6	393.7 $\pm$ 1.6	394.9
μ	350.5 $\pm$ 14.5	354.8 $\pm$ 3.1	354.7 $\pm$ 3.0	353.7
m_t	171.4 $\pm$ 1.0	171.4 $\pm$ 0.12	171.4 $\pm$ 0.12	171.4

Table 3: Result for the general MSSM parameter determination in SPS1a assuming flat theory errors. As experimental measurements the kinematic endpoint measurements are used for the LHC column, and the mass measurements for the ILC column. In the LHC+ILC column these two measurements sets are combined. Shown are the nominal parameter values and the result after fits to the different data sets. All masses are given in GeV.

Of course, one can *assume* the mSUGRA boundary conditions. In this case, the errors on the GUT-scale values are (hep-ph/0410364):

	LHC	ILC	LHC+ILC
Δm_0	$\mathbf{4.0}$ GeV	$\mathbf{0.09}$ GeV	$\mathbf{0.08}$ GeV
$\Delta m_{1/2}$	$\mathbf{1.8}$ GeV	$\mathbf{0.13}$ GeV	$\mathbf{0.11}$ GeV

Table 4: Errors using masses, including errors, as input. For LHC, using edges/endppoints directly reduces errors — see next table.

	SPS1a	$\Delta^{\mathrm{theo-exp}}_{\mathrm{zero}}$	$\Delta^{\mathrm{expNoCorr}}_{\mathrm{zero}}$	$\Delta^{\mathrm{theo-exp}}_{\mathrm{zero}}$	$\Delta^{\mathrm{theo-exp}}_{\mathrm{gauss}}$	$\Delta^{\mathrm{theo-exp}}_{\mathrm{flat}}$
		masses	endpoints			
m_0	100	4.11	1.08	0.50	2.97	2.17
$m_{1/2}$	250	1.81	0.98	0.73	2.99	2.64
$\tan\beta$	10	1.69	0.87	0.65	3.36	2.45
A_0	-100	36.2	23.3	21.2	51.5	49.6
m_t	171.4	0.94	0.79	0.26	0.89	0.97

Table 5: Best–fit results for MSUGRA at the LHC derived from masses and endpoint measurements with absolute errors in GeV. The big columns correspond to mass and endpoint measurements. The subscript represents neglected, (probably approximate) gaussian or proper flat theory errors. The experimental error includes correlations unless indicated otherwise in the superscript. The top mass is quoted in the on-shell scheme.

	SPS1a	$\Delta_{\text{endpoints}}$	Δ_{ILC}	$\Delta_{\text{LHC+ILC}}$	$\Delta_{\text{endpoints}}$	Δ_{ILC}	$\Delta_{\text{LHC+ILC}}$
		exp. errors			exp. and theo. errors		
m_0	100	0.50	0.18	0.13	2.17	0.71	0.58
$m_{1/2}$	250	0.73	0.14	0.11	2.64	0.66	0.59
$\tan\beta$	10	0.65	0.14	0.14	2.45	0.35	0.34
A_0	-100	21.2	5.8	5.2	49.6	12.0	11.3
m_t	171.4	0.26	0.12	0.12	0.97	0.12	0.12

Table 6: Best–fit results for MSUGRA at the LHC (endpoints) and including ILC measurements. Only absolute errors are given. The LHC results correspond to Tab. 5, including flat theory errors.

The absolute mass scale accuracies from the LHC are not so bad if one assumes mSUGRA, but to prove mSUGRA we would like to do better than the results shown in Tables 2 and 3.

Summary

For getting high accuracy for Ω_χ and the GUT-scale $M_{1,2,3}$ and other parameters without assuming mSUGRA, it is highly desirable to improve absolute mass accuracies obtained from LHC data alone.

We have developed some techniques that give mass accuracies at least as

good as claimed in the ATLAS mass-edge study, using some very different techniques.

The first to be described is sort of a "super-edge" technique.

The second is a "direct solution" technique in which a few events are used to directly solve for the masses.

Both techniques are such that if there were no experimental effects, no combinatoric issues, ... then exact values for all masses in the SPS1a (or similar) decay chain could be obtained.

General Strategy:

- **One would like to use pure kinematics to get the absolute masses,** *i.e.* **not use cross sections, momentum correlations,** *etc.*, **which are are presumably quite model dependent.**
- **Then, once the masses are known one can input these into the various possible models and much more reliably employ cross sections, correlations and so forth to discriminate between models.**

Basic Constraint Counting

One chain examples

1. The "marginal" case is 3 visible particles (or combinations of particles) with 3 on-shell resonances involved and 1 final invisible particle:

   $$Z \to Y v_1 \to X v_2 v_1 \to N v_3 v_2 v_1 \tag{4}$$

   For this case, after n events, the number of unknowns is 4 masses and $4n$ 4-momenta of the final invisible particle (N).

   The number of on-shell constraints from requiring given Z, Y, X, N masses in each event is $4n$.

   Thus, the number of unknowns is always $4 + 4n - 4n = 4$ (the masses) no matter how many events.

2. For 4 visible particles with 4 on-shell resonances and the final N, after n events there are $5 + 4n$ unknowns and $5n$ constraints, implying equality

when $n = 5$. So, if there were no combinatoric / resolution issues, $n = 5$ events would allow you to solve for the 5 masses aside from discrete quartic equation solution ambiguities.

Two chain examples

1. The "marginal" case here is just two visible particles per chain: $Y \to X v_1 \to N v_2 v_1$.

   If we assume equal masses on the two chains, then there are 3 unknown masses, including m_N.

   For each event, there are the two 4-momenta of the two final N's, but we know the sum of their transverse momenta from balancing against the visible particle transverse momenta, implying 6 unknown momenta components per event.

   After n events, the number of unknowns is then $3 + 6n$.

   The number of constraints is $6n$ (since we assume on-shell masses on both chains.)

   Thus, no matter how many events, we always have the 3 unknown mass parameters that cannot be absolutely solved for.

Note that by considering both chains, we are at the marginal situation with just 2 visible particles and 2 on-shell resonances plus the 1 final invisible particle, as opposed to the one-chain case where marginality required 3 visible particles, corresponding to 3 on-shell resonances plus 1 invisible particle.

2. The first non-marginal case is clearly 3 visible particles *per chain*, corresponding to $3 + 1 = 4$ unknown masses.

   In this case, after n events we have $4 + 6n$ unknowns and $8n$ on-shell constraints (recall we have two chains each of which has four mass constraints) implying solution (subject to discrete ambiguities) when $4 + 6n - 8n = 0 \Rightarrow n = 2$.

   Again, there is a reduction in the number of on-shell resonances and associated visible particles that are needed to get discrete solutions, as compared to considering a single chain.

A significant problem with both the 1-chain and 2-chain approaches is combinatorics.

For example, for the decay chain $\widetilde{q} \to q\widetilde{\chi}_2^0 \to q\mu\widetilde{\mu}_R \to q\mu\mu\widetilde{\chi}_1^0$ in $\widetilde{q}\widetilde{q}$ production, in each event there would be $2!$ ways to place the q's and

$4 \times 2 \times 2$ ways to place the μ's (noting that each chain has to have one μ^+ and one μ^-, but we don't know which comes first.) The net is $2 \times 16 = 32$ ways of placing particles.

If there are additional jets from ISR and / or from $\widetilde{g}\widetilde{q}$ and $\widetilde{g}\widetilde{g}$ production, there would be additional combinatoric possibilities or else one would need to implement a selection criterion for choosing the jets that one hoped came from $\widetilde{q}$ decays directly.

Advantages and Disadvantages of 1-chain vs. 2-chain approaches.

1-chain:

Less combinatoric ambiguity if you can isolate events in which there are e.g. exactly two leptons, implying that the other side of the event is "simple".

But, must go deeper into the chain to get an equivalent level of constraint (3 visible particles in the chain vs. 2 in minimal cases).

2-chain:

More combinatoric ambiguity (assuming the two chains are the same as in the analyses to be discussed).

But, need not go as deeply into the chain in the minimal case and need fewer events to "solve" in the first solvable situation (2 events vs. 5 events — the 5 events in the 1-chain case, means a high multiplicity of solutions which may more than offset gain on combinatorics).

$\mathbf{2}$ chains — $\mathbf{2}$ visible particles per chain

- **We claim that one can do well at the LHC by taking the more global point of view and using as much information as is available in every event.**

  Our approach can be applied to many different types of event topologies, but here we focus on a subcomponent of the SPS1a type event in a way that has not been previously attempted.

  Consider the chain decay sequence:

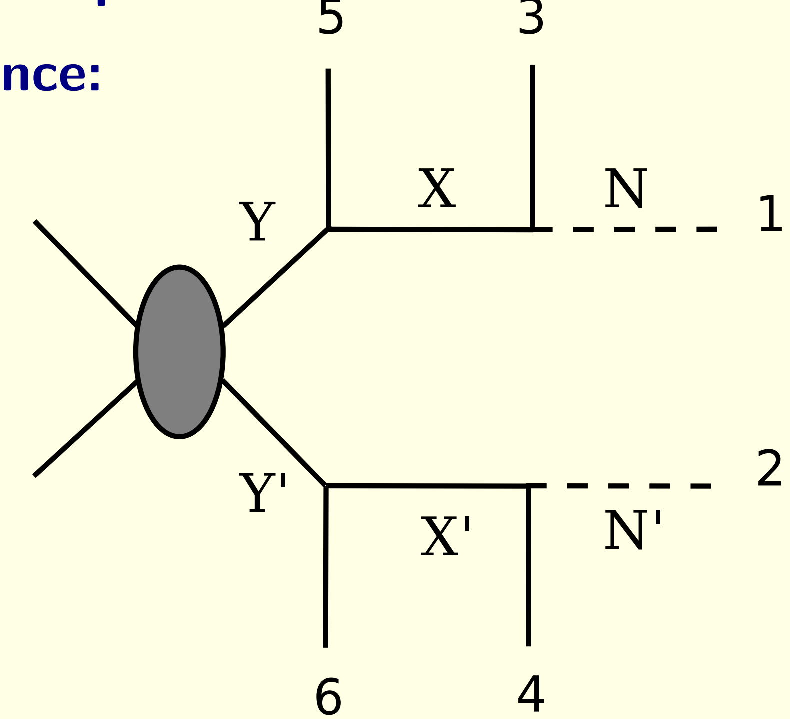

Figure 2: *A typical chain decay topology.*

Note: some cuts to isolate a given topology are required (just as in the previous analyzes) — perhaps OSET would do the job. By this, we don't mean perfect isolation — roughly a ratio of $S/B > 2$ is certain to work, where B could include old physics and new physics signals of other topologies. Even $S/B \sim 1$ is probably workable.

This topology can be applied to many processes with 4 visible and 2 invisible particles.

For example, suppose $M_Y = M_{Y'}$, $M_X = M_{X'}$, and $M_N = M_{N'}$.

Examples that fit this:

$$
\begin{aligned}
t\bar{t} &\rightarrow bW^+bW^- \rightarrow bl^+\nu bl^-\bar{\nu} \\
\tilde{\chi}_2^0\tilde{\chi}_2^0 &\rightarrow l\tilde{l}l\tilde{l} \rightarrow ll\tilde{\chi}_1^0 ll\tilde{\chi}_1^0 \\
\tilde{q}\tilde{q} &\rightarrow q\tilde{\chi}_2^0 q\tilde{\chi}_2^0 \rightarrow ql\tilde{l}ql\tilde{l} \rightarrow qll\tilde{\chi}_1^0 qll\tilde{\chi}_1^0 \\
\tilde{t}\bar{\tilde{t}} &\rightarrow b\tilde{\chi}^+\bar{b}\tilde{\chi}^- \rightarrow bW^+\tilde{\chi}_1^0\bar{b}W^-\tilde{\chi}_1^0
\end{aligned}
$$

The third entry above is the SPS1a case of interest.

Let us count the constraints and unknowns once again. For this we (temporarily) assume that the particles are exactly on-shell and that experimental resolutions are perfect.

1. **There are 8 unknowns corresponding to the 4-momenta of the N and N'.**

2. **There are 2 constraints on these coming from knowledge of the visible transverse momenta. (We are assuming that the longitudinal momentum and energy of the collision is not known, as appropriate at a hadron collider.)**

   If there are extra visible jets in the event we just include them in visible $\vec{p}_T$.

   The visible particles 3, 4, 5 and 6 need not be stable. We just need to be able to determine their 4-momenta (e.g. $W \to jj$ is ok but $W \to \ell\nu$ is not).

3. **There are the 3 constraints coming from requiring the equalities: $M_Y = M_{Y'}$, $M_X = M_{X'}$, and $M_N = M_{N'}$.**

4. **Thus, for each event, since $(8-2)-3=3$ we see that if we know the 3 masses, then we can solve for the 4-momenta of the N and N' and vice versa.**

The equations are quartic, and so there can be 4, 2 or 0 solutions (with acceptable positive real energies for the N and N'). If not 0, then the event is "solved" for those particular mass choices.

5. For each event, we scan through the mass space to see if one or more of the discrete solutions is acceptable.

   Each event then defines a 3-dimensional region in the 3-dimensional mass space that is physically acceptable.

6. As we increase the number of events the 3-dimensional mass region consistent with all events becomes smaller.

   However, in general (and in practice) this region will not shrink to a point.

   Thus, we need additional methods to pick out the correct point in mass space.

- To illustrate our approach, we can consider the explicit example

$$\begin{array}{c} \widetilde{\chi}_2^0\widetilde{\chi}_2^0 \to \ell\widetilde{\ell}\ell\widetilde{\ell} \to \ell\ell\widetilde{\chi}_1^0\ell\ell\widetilde{\chi}_1^0 \\ i.e. \quad Y = Y' = \widetilde{\chi}_2^0, \quad X = X' = \widetilde{\ell}, \quad N = N' = \widetilde{\chi}_1^0, \end{array},$$

which we generate as a subcomponent of

$$\tilde{q}\tilde{q} \to q\tilde{\chi}_2^0 q\tilde{\chi}_2^0 \to \ldots \to q\ell\ell\tilde{\chi}_1^0 q\ell\ell\tilde{\chi}_1^0 . \tag{5}$$

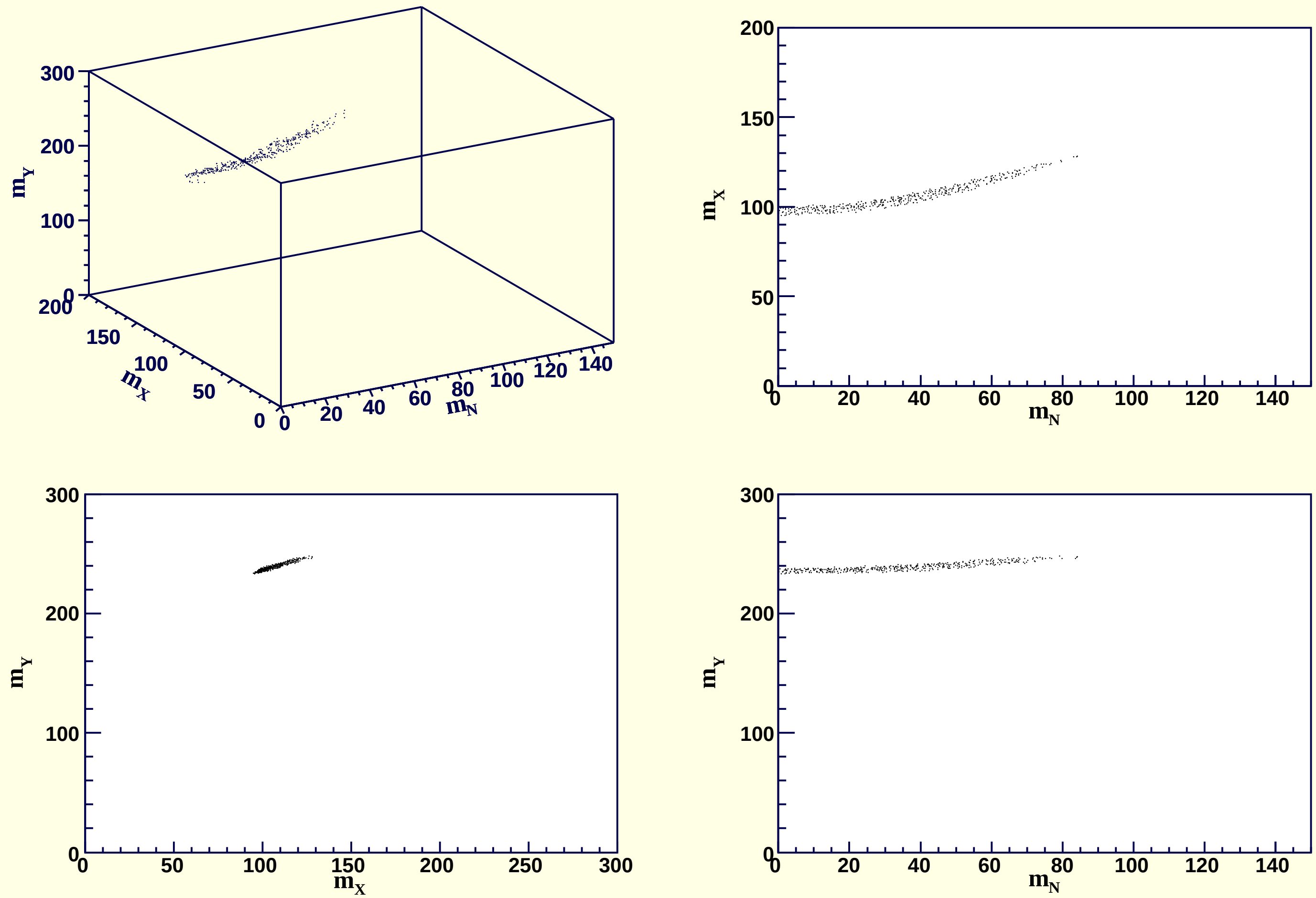

Figure 3: *Mass region (in GeV) that can solve all events.* $\mathbf{500}$ *generated events for* $m_Y = 246.6$ GeV, $m_X = 128.4$ GeV *and* $m_N = 85.3$ GeV, *using correct chain assignments and perfect resolution. Masses from 'Model I', with large* $m_{\tilde{\chi}_2^0}$.

We found that the correct masses lie at the end point of the allowed region. A graphical picture is:

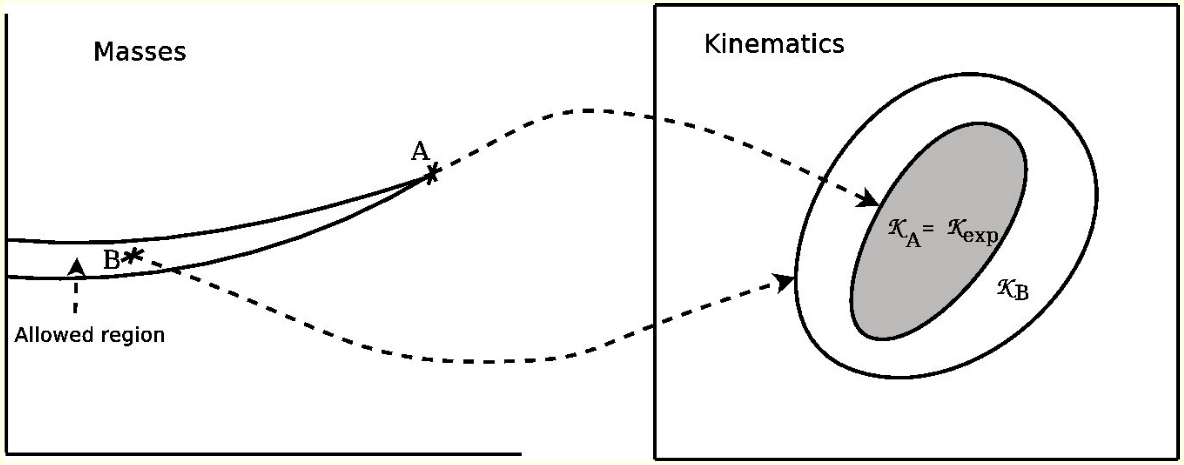

Figure 4: *Map between mass space and kinematic space. The nominal masses, point $\boldsymbol{A}$, produces a kinematic region that coincides with the experimental region: $\mathcal{K}_{\boldsymbol{A}} = \mathcal{K}_{\boldsymbol{exp}}$. A point $\boldsymbol{B}$ inside the allowed mass region produces a larger kinematic region: $\mathcal{K}_{\boldsymbol{B}} \supset \mathcal{K}_{\boldsymbol{exp}}$.*

The kinematic space $\mathcal{K}$ refers to the set of observable momenta of the 4 leptons in the chain.

The allowed masses in $\mathcal{M}$ space are those for which every point in the $\mathcal{K}_{exp}$ part of $\mathcal{K}$ space produces at least one acceptable set of $\vec{p}_N$ and $\vec{p}_{N'}$, $i.e.$ is 'solved'.

a) The correct set of masses, $\mathcal{M}$ at point A in Fig. 4, produces a kinematic region $\mathcal{K}_A$ that coincides with the experimental one, $\mathcal{K}_A = \mathcal{K}_{exp}$, as long as the experimental statistics is large enough.

b) A different mass point produces a region that is either smaller or larger than $\mathcal{K}_{exp}$[1].

c) If smaller, the mass point does not appear in the mass region for which **all** events are solved.

d) If larger, all events are solved; we denote this kind of point, with mass set $\mathcal{M}'$, as point B in Fig. 4.

e) Let us shift the masses slightly to $\mathcal{M}' + \delta\mathcal{M}'$.

- If the kinematic region for which we have acceptable solutions still covers $\mathcal{K}_{exp}$, then $\mathcal{M}' + \delta\mathcal{M}'$ is still within the allowed region.
- Apparently, point B, which produces a region larger than K_{exp}, has the freedom to move in all directions and must live inside the allowed region.
- On the other hand, the correct mass point A, which produces exactly $\mathcal{K}_{exp}$, has the least freedom to move and must be located at an end point of the allowed region.

However, with finite resolutions and combinatorics (which lepton goes where

[1] In general cases, there could exist degenerate points that produce exactly the same kinematic region as the correct one. It is impossible to raise the degeneracy using pure kinematics.

in the two chains), not all events can be solved by the correct mass point.

$\Rightarrow$ The correct mass point will not lie within the intersection region (assuming there is any such region left).

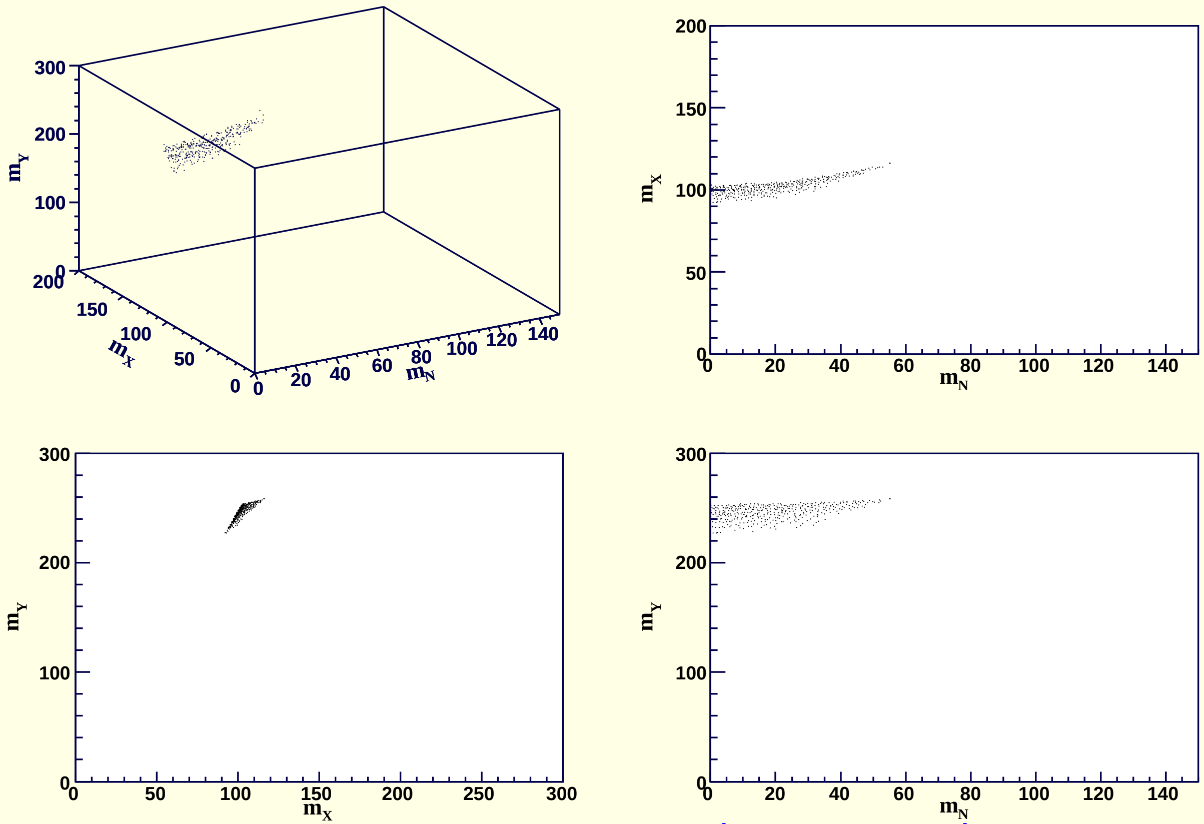

Figure 5: *The allowed mass region (in* GeV*) with smearing (ALTFAST) and wrong combinatorics.* $\mathbf{500}$ *generated events for Model I masses:* $\boldsymbol{m_Y} = \mathbf{246.6}\ \mathrm{GeV}, \boldsymbol{m_X} = \mathbf{128.4}\ \mathrm{GeV}$ *and* $\boldsymbol{m_N} = \mathbf{85.3}\ \mathrm{GeV}$*. Cuts:* $|\boldsymbol{\eta}| < \mathbf{2.5}$, $\boldsymbol{p_T(\ell)} > \mathbf{6}\ \mathrm{GeV}$.

- In the more realistic case, the correct mass choices do not correspond to an endpoint but rather correspond to the choices such that changes in the masses result in the most rapid decline in the number of solved/consistent events.

- Looking for this point of steepest decline in a 3-dimensional space is numerically difficult.

- If we fix two of the masses, and vary the $3rd$ mass, then we can usually identify the point at which the number of solved events starts a steep decline as this $3rd$ mass is changed.

  This will allow an iterative approach.

- The approach that works is to cycle through the $3rd$-mass choices, m_N, m_X and m_Y in that order, and at each stage look for the peak in the number of solved/consistent events as a function of the m_N mass each time it is the $3rd$-mass. Then, update this $3rd$-mass to the peak location.

  The 'peaks' are actually obtained by the intersection of the two fitted straight lines illustrated in the following figure, where two masses are set to their correct values and the $3rd$-mass is varied.

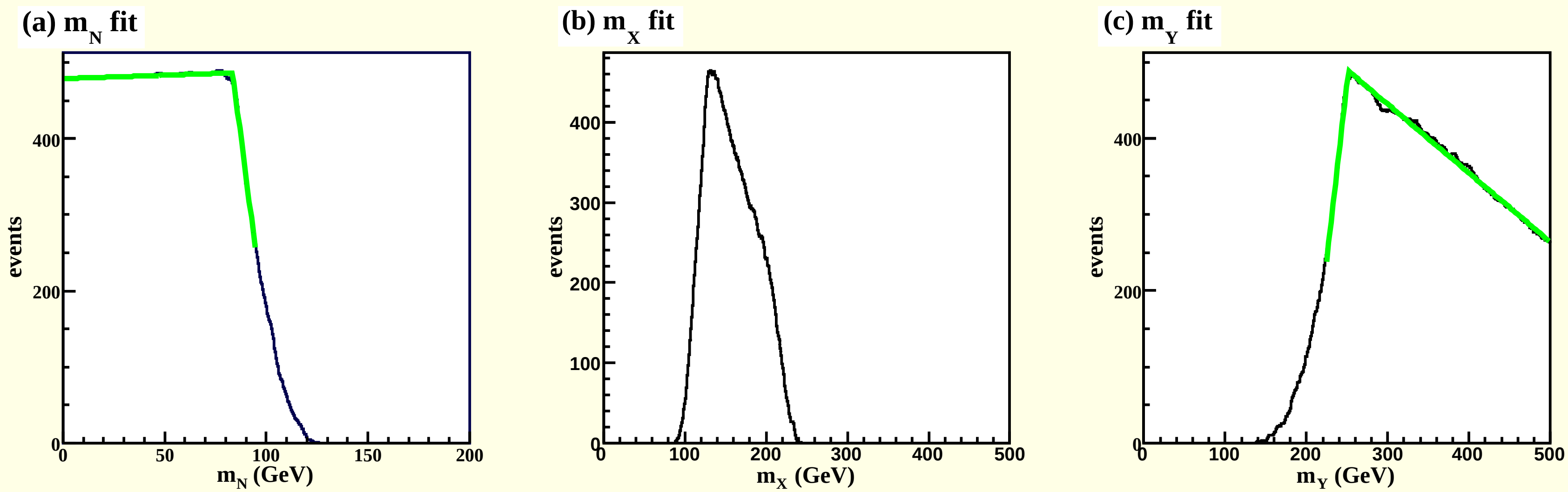

Figure 6: *One-dimensional fits by fixing the other two masses at the correct values. 500 events, combinatorics, smearing and simple cuts included. Peaks are close to correct masses.*

- **We now get more realistic. For certain soft-SUSY parameters one obtains our Model I with**

$$m_{\widetilde{g}} \sim 524, \quad m_{\widetilde{d}_L,\widetilde{s}_L} \sim 438, \quad m_{\widetilde{u}_L,\widetilde{c}_L} \sim 431$$
$$m_{\widetilde{\chi}_2^0} \sim 246.6, \quad m_{\widetilde{\mu}_R} \sim 128.4, \quad m_{\widetilde{\chi}_1^0} \sim 85.3 \tag{6}$$

For this point, the net cross section available is

$$\sigma\left(pp\to\sum_{q,q'=u,d,c,s}\widetilde{q}_L\,\widetilde{q}'_L+\sum_{q,q'=u,d,c,s}\widetilde{q}_L\,\overline{\widetilde{q}'_L}+\sum_{q,q'=u,d,c,s}\overline{\widetilde{q}_L}\,\overline{\widetilde{q}'_L}\right)\sim 2.9\times 10^4\ \mathrm{fb}\,, \tag{7}$$

coming from all sources including gg fusion, $u_L u_L$ fusion, *etc.* The branching ratios relevant to the particular decay chain we examine are

$$\begin{aligned} &B(\widetilde{q}_L\to q\widetilde{\chi}^0_2)\sim 0.27 \quad (q=u,d,c,s)\\ &B(\widetilde{\chi}^0_2\to\widetilde{\mu}^\pm_R\mu^\mp)\sim 0.124\\ &B(\widetilde{\mu}^\pm_R\to\mu^\pm\widetilde{\chi}^0_1)=1\,. \end{aligned} \tag{8}$$

The net effective branching ratio for the double decay chain is

$$B(\widetilde{q}_L\widetilde{q}_L\to 4\mu\widetilde{\chi}^0_1\widetilde{\chi}^0_1)\sim(0.27)^2\times(0.124)^2\sim 1.12\times 10^{-3} \tag{9}$$

for any one $\widetilde{q}_L$ choice. The effective cross section for the $4\mu\widetilde{\chi}^0_1\widetilde{\chi}^0_1$ final state is then

$$\sigma(4\mu\widetilde{\chi}^0_1\widetilde{\chi}^0_1)\sim 2.9\times 10^4\ \mathrm{fb}\times 1.12\times 10^{-3}\sim 32.5\ \mathrm{fb}\,. \tag{10}$$

For an integrated luminosity of $L = 90\ \mathrm{fb}^{-1}$, this gives us 2900 $4\mu\widetilde{\chi}_1^0\widetilde{\chi}_1^0$ events before any cuts are applied.

Initial and final state radiation, resonance widths, combinatorics and experimental resolutions (as in ATLFAST) are all included.

To reduce the SM background, we require that all muons are isolated and pass the kinematic cuts:

$$|\eta|_\mu < 2.5, \quad P_{T\mu} > 10\ \mathrm{GeV}, \quad \not{p}_T > 50\ \mathrm{GeV}. \tag{11}$$

With these cuts, the four-muon SM background is negligible.

The number of signal events is reduced from 2900 to about 1900.

The procedure comprises the following steps:

1. Randomly select masses $m_Y > m_X > m_N$ that are below the correct masses (for example, the current experimental limits).
2. Plot the number of solved events, N_{evt}, as a function of one of the 3 masses in the recursive order m_N, m_X, m_Y with the other two masses fixed. In the case of m_Y and m_N, we fit N_{evt} for the plot with two straight lines and adopt the mass value at the intersection point as the updated mass. In the case of m_X, the updated mass is taken to be the mass at the peak of the N_{evt} plot.

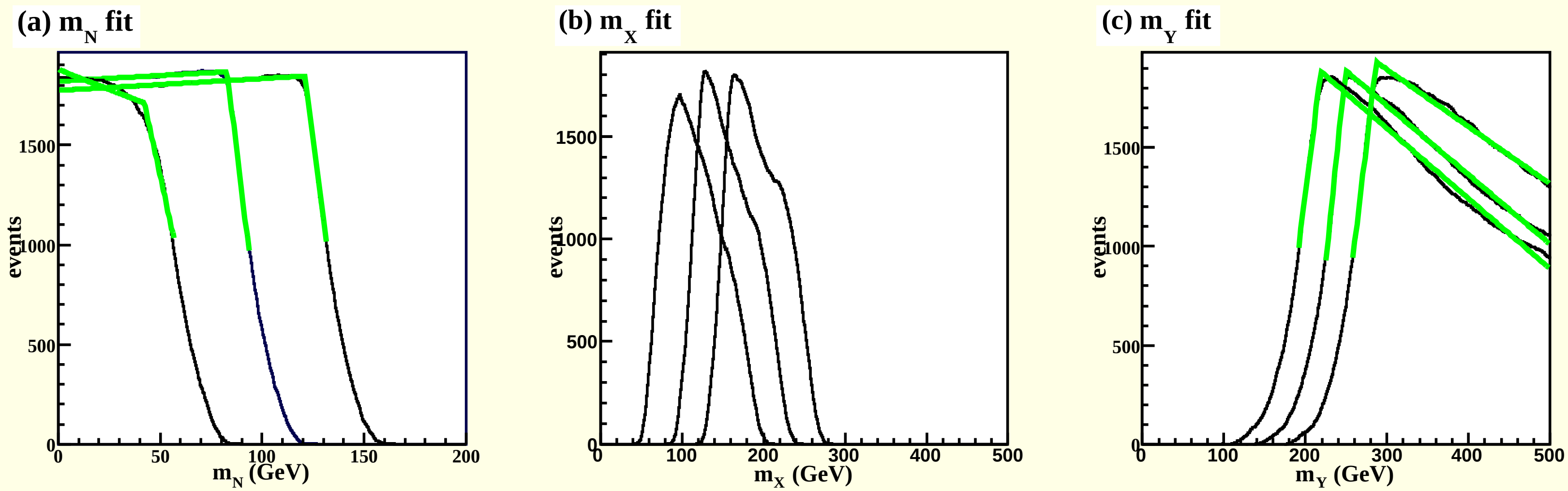

Figure 7: *A few steps showing the migration of the one dimensional fits. The middle curve in each plot corresponds to masses close to the correct values.*

A few intermediate one-dimensional fits are shown in Fig. 7.

3. **Each time after a fit to m_N, record the number of events at the intersection (sometimes called the turning point) of the two straight lines, as exemplified in Fig. 7 a. This event number at the turning point will in general be non-integer.**
4. **Repeat steps 2 and 3. The number of events recorded in step 3 will in general increase at the beginning and then decrease after some steps, as seen in Fig. 8. Halt the recursive procedure when the number of (fitted) events has sufficiently passed the maximum position.**
5. **Fit Fig. 8 to a (quartic) polynomial and take the position where the polynomial is maximum as the estimated m_N.**
6. **Keep m_N fixed at the value in step 5 and do a few one-dimensional fits**

for m_Y and m_X until they are stabilized. Take the final values as the estimates for m_Y and m_X.

- The end result is the plot below.

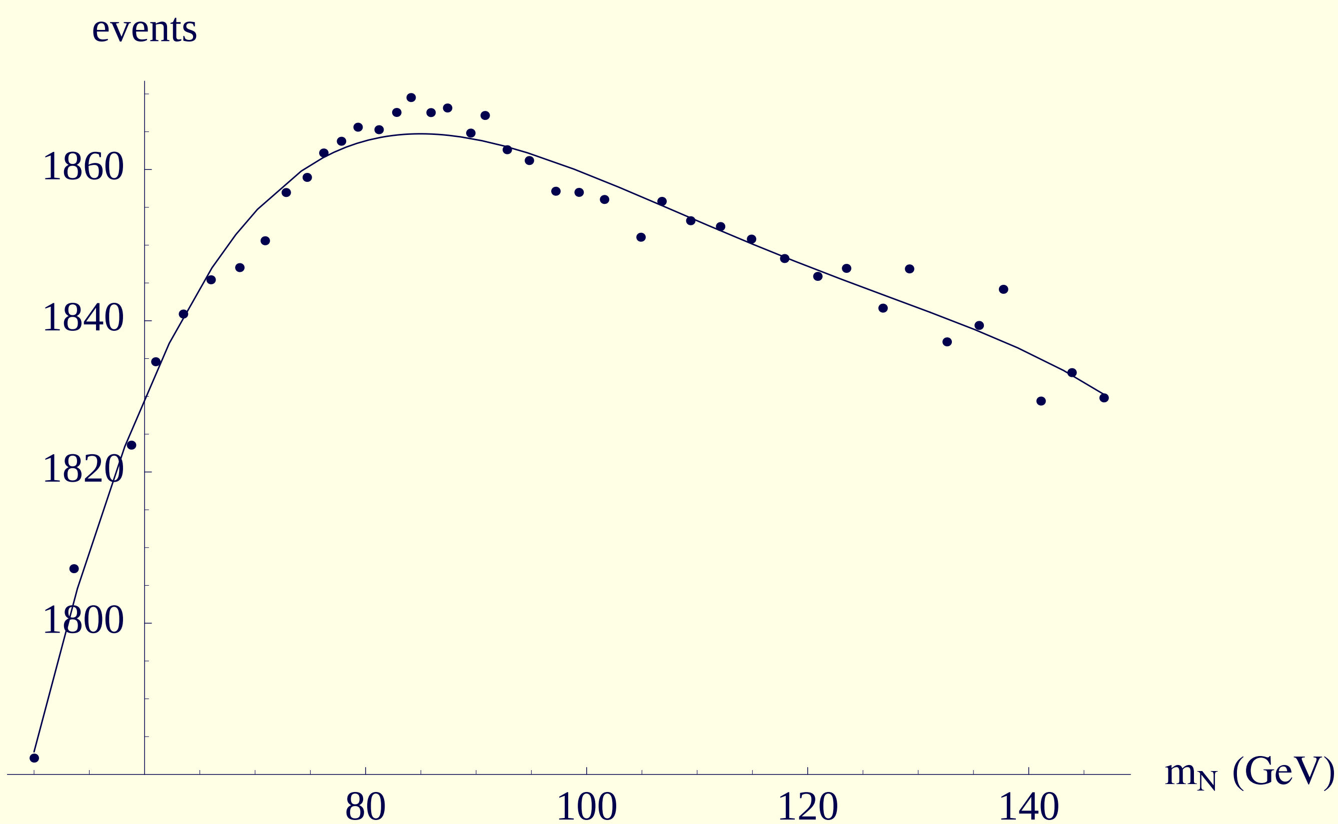

Figure 8: *The final plot for determining m_N. The position of the maximum of the fitted polynomial is taken to be the estimation of m_N..*

Remarkably, the point at which the turnover occurs gives M_N (and M_X

and M_Y) to good accuracy.

The final values for the masses in one "experiment" were determined as

$$\{252.2, 130.4, 85.0\}\ \mathrm{GeV} \quad vs. \quad \{246.6, 128.4, 85.3\}\ \mathrm{GeV} \tag{12}$$

Remarkably, the N mass is extremely accurate and the Y mass quite close as well.

A deeper understanding of our procedure can be gained by examining the graphical representation of the steps taken in the (m_Y, m_N) plane shown in Fig. 9.

There, we display contours of the number of (fitted) events after maximizing over possible m_X choices.

There is a 'cliff' of falloff in the number of solved events beyond about 1825 events. It is the location where this cliff is steepest that is close to the input masses, which are indicated by the (red) star.

The mass obtained by our recursive fitting procedure is indicated by the (blue) cross.

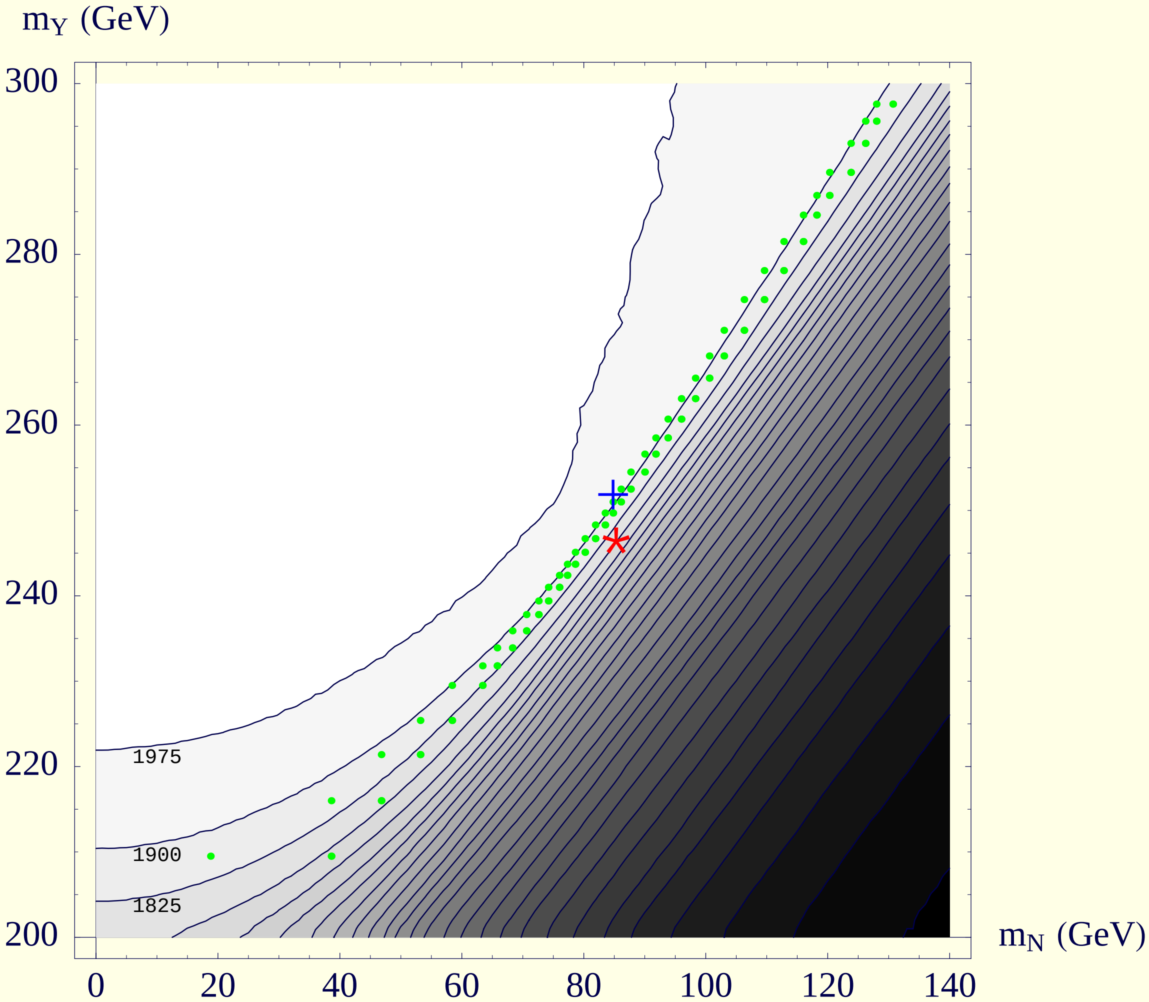

Figure 9: *Contours for the number of solved events in the* $\boldsymbol{m_N \sim m_Y}$ *plane with 2000 events. The number of events is the maximum value obtained after varying* $\boldsymbol{m_X}$*. Contours are plotted at intervals of 75 events, beginning with a maximum value of 1975. The green dots correspond to a set of one-dimensional fits. The* ⋆ *shows the input masses and the* + *shows our fitted masses.*

- **Error evaluation:**

Must adopt an 'experimental' approach for such an empirical procedure:

Generate 10 different $90\ \mathrm{fb}^{-1}$ data samples and apply the procedure to each sample.

Estimate the errors of our method by examining the statistical variations of the 10 samples, which yields

$$m_Y = 252.2 \pm 4.3\,\mathrm{GeV}, \quad m_X = 130.4 \pm 4.3\,\mathrm{GeV}, \quad m_N = 86.2 \pm 4.3\,\mathrm{GeV}. \tag{13}$$

The statistical variations for the mass differences are much smaller:

$$\Delta m_{YX} = 119.8 \pm 1.0\,\mathrm{GeV}, \quad \Delta m_{XN} = 46.4 \pm 0.7\,\mathrm{GeV}. \tag{14}$$

Compared with the correct values $\mathcal{M}_A = \{246.6, 128.4, 85.3\}$, we observe small biases in the mass determination, which means that our method has some "systematic errors".

However, these systematic errors are determined once we fix the experimental resolutions, the kinematic cuts and the fit procedure.

Therefore, they can be easily corrected for, which leaves us errors for the absolute mass scale of $\sim few\ \mathrm{GeV}$ and for the mass differences of $\sim \mathbf{1}\ \mathrm{GeV}$ which will decrease further after adding in $2e2\mu$ and $4e$ final states.

- $\boxed{\text{Backgrounds}}$

In the above example, the background is negligible with the applied cuts.

However, if in some other case the backgrounds turned out to be substantial, they could decrease the accuracy of the mass determination.

Instead of analyzing another process with sizable backgrounds, we stick to the four muon events studied above but make up more “backgrounds”.

In particular, we consider the 4-muon events from top pair production, but unlike above we do not require the muons to be isolated (which eliminates this background).

$\Rightarrow$ a significant number of events have 4 hard muons.

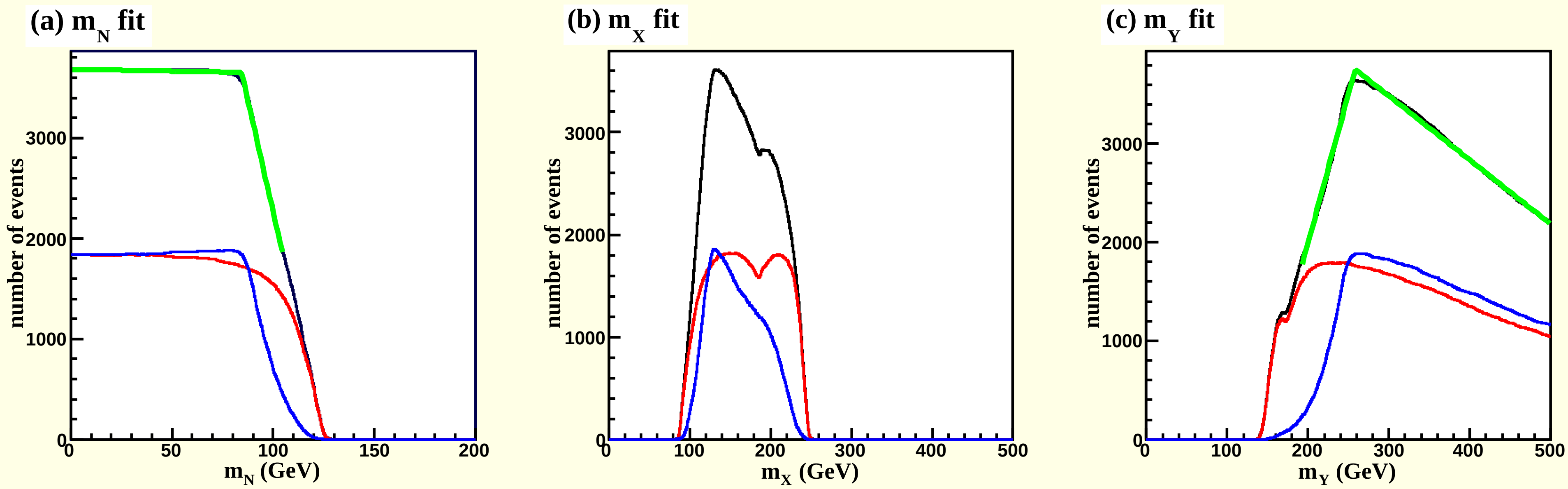

Figure 10: *Fits with $90 fb^{-1}$ signal events and an equal number of background events. Separate numbers of signal (blue) and background (red) events are also shown.*

Adding an equal number of background events to $90 fb^{-1}$ signal events, we repeat the one-dimensional fits. A typical cycle around the correct masses is shown in Fig. 10.

For comparison the number of solvable signal events and background events are also shown separately.

The effect of background events is clear: the curve for solvable background

events is much smoother around the turning point, and therefore smears but does not destroy the turning point.

Although we are considering one specific background process, this effect should be generic, unless the backgrounds happen to have non-trivial features around the turning points.

Nevertheless, due to the fact that there are 8 possible combinations, the chance that a background event gets solutions is quite large and they do affect the errors and biases of the mass determination.

This can be seen in Fig. 11, in which we have used the same 10 sets of signal events as in the previous subsection, but varied the number of background events according to the ratio $background/signal = 0, 0.1, 0.2, 0.5, 1$.

We observe increases in both the biases and variations.

But, if the backgrounds are understood (which if SM, they will be), then we can correct for them.

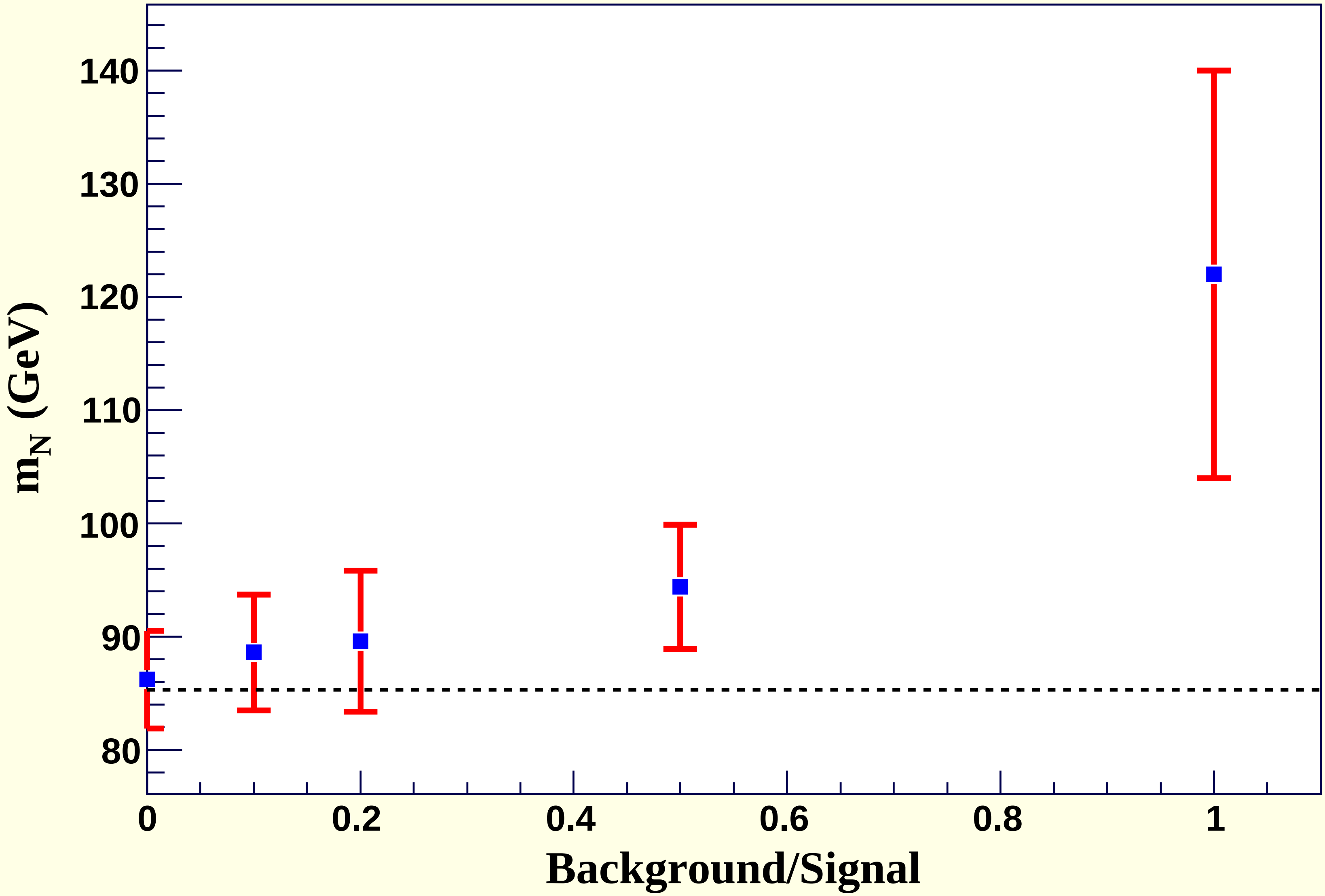

Figure 11: m_N *determination with different background-signal ratio. The dashed horizontal line corresponds to the correct* m_N.

- **If it should be that $m_N \sim 0$, then we will know it.**

  We have found that it would quickly become apparent that we were not finding a maximum in the included event number as m_N is increased.

  We would then backtrack to $m_N = 0$ and find that actually the number of included events is largest there and declines as m_N increases. A typical plot is shown in Fig. 12.

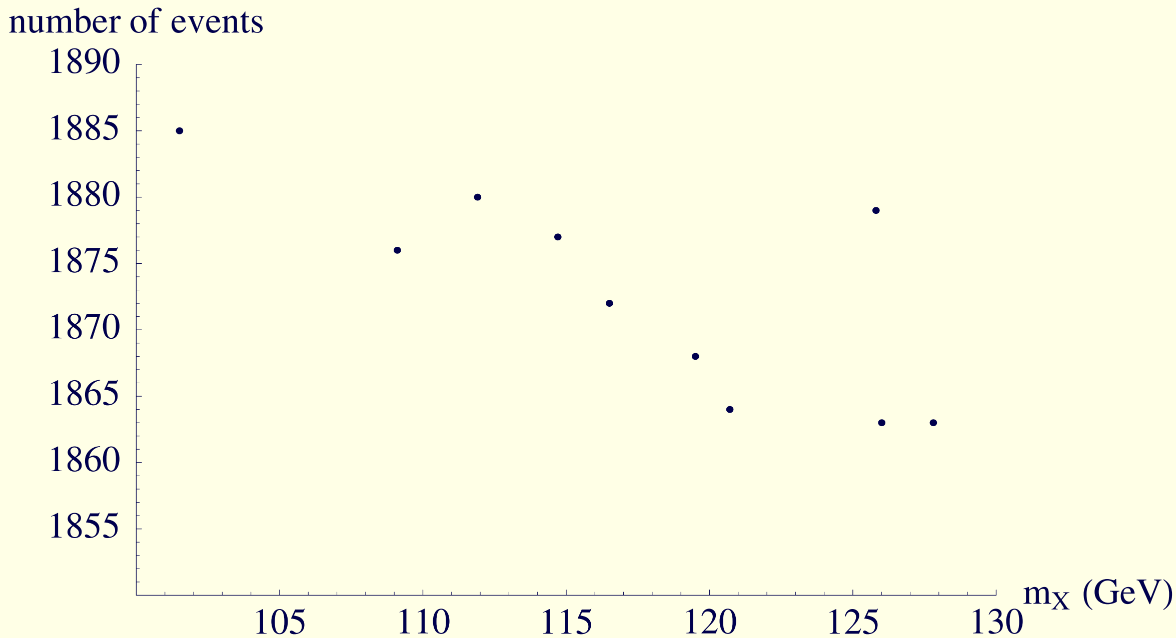

Figure 12: *m_N determination for a case with $m_Y = 199.4$ GeV, $m_X = 100$ GeV and $m_N = 0.1$ GeV. Requires very large μ in SUSY model. 2000 event sample.*

- **Peculiar mass separation choices can give some special features.**

  We are currently working on optimizing our procedures for such cases.

- **We are confident that the experimental groups will actually end up doing even better in the end.**

  In particular, if they understand the backgrounds then they can separately apply our procedure to them and subtract the background from the summed curves of Fig. 10, returning us to a situation close to the zero-background case first considered.

The SPS1a Point

- **It is desirable to compare directly to the results obtained by others for the SPS1a SUSY parameter point.**

- **We perform the analysis using the same $4\mu\widetilde{\chi}_1^0\widetilde{\chi}_1^0$ final state that we have been considering. For the usual SPS1a mSUGRA inputs the masses for $Y = \widetilde{\chi}_2^0$, $X = \widetilde{\mu}_R$ and $N = \widetilde{\chi}_1^0$ (from ISAJET 7.75) are 180.3 GeV, 142.5 GeV and 97.4 GeV, respectively.**

- **This is a more difficult case than Point I considered earlier due to the fact that the dominant decay of the $\widetilde{\chi}_2^0$ is $\widetilde{\chi}_2^0 \to \tau\widetilde{\tau}_1$. The branching ratio for $\widetilde{\chi}_2^0 \to \mu\widetilde{\mu}_R$ is such as to leave only about 1200 events in the $4\mu\widetilde{\chi}_1^0\widetilde{\chi}_1^0$ final state after $L = 300~\mathrm{fb}^{-1}$ of accumulated luminosity.**

- **Cuts reduce the number of events further to ~ 425.**

  This is too few for our technique to be as successful as for the case considered earlier.

- **After including combinatorics and resolution we obtain:**

$$m_Y = 188 \pm 12~\mathrm{GeV}\,, \quad m_X = 151 \pm 14~\mathrm{GeV}\,, \quad m_N = 100 \pm 13~\mathrm{GeV}\,. \tag{15}$$

  In Fig. 13, we give an SPS1a plot analogous to Fig. 8.

  Errors are determined by generating many such plots for different samples of ~ 425 events (the exact number changes depending upon event details).

  Errors will come down to about $\pm 5~\mathrm{GeV}$ after including $2e2\mu$ and $4e$ final states, making our results comparable to the ATLAS LHC edge results.

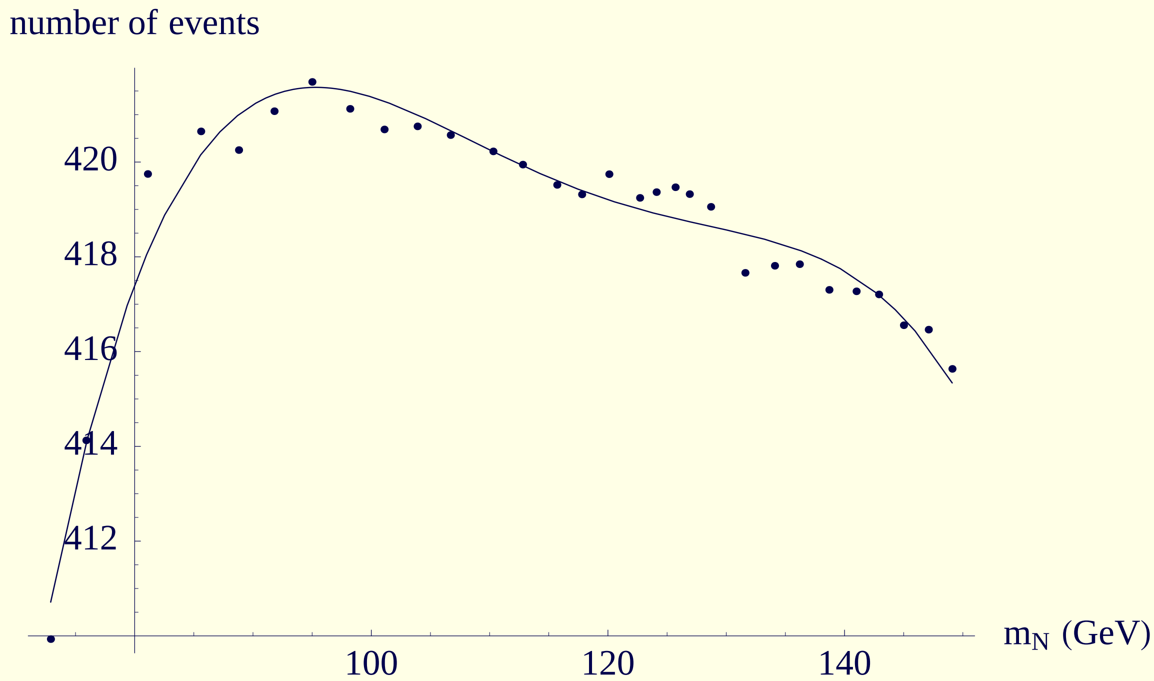

Figure 13: *Fitted number of events at the turning point as a function of m_N for the fits for the SPS1a case.*

Note the vertical scale. The change in the number of events as one varies m_N is quite small for small event samples and this is what leads to the larger errors in this case, when considering just the 4μ final state.

- **In principle, we must also take into account the fact that the dominant $\widetilde{\chi}_2^0 \to \tau\widetilde{\tau}_1$ decays provide a background to the purely muonic final state.**

The background level (after cuts and branching ratios) is at about the 50% level. However, using other channels involving e's to which it, but not our signal, contributes, we can subtract this background statistically.

We have not yet performed the relevant procedure to see how well we do, but we expect that the net background contamination will be equivalent to $B/S \lesssim 0.1$, a level for which our techniques work very well and the errors quoted earlier for the SPS1a point will not be increased by very much.

$\mathbf{2}$ chains: $\mathbf{3}$ visible particles per chain

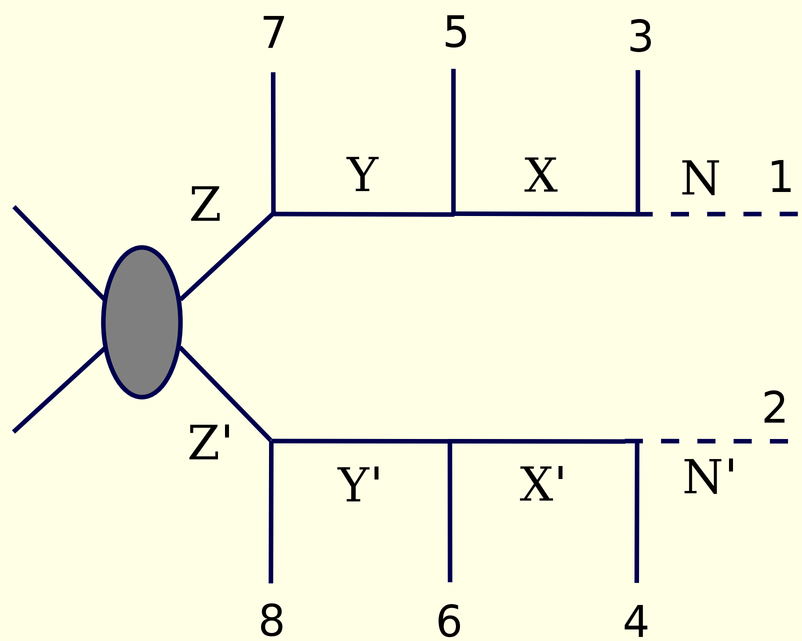

Figure 14: The 3-visible per chain topology.

- **Recall from the counting section that to solve requires just $n = 2$ events.**

  Assuming we can isolate LHC events with the topology in Fig. 14 and using $m_N = m_{N'}$, $m_X = m_{X'}$, $m_Y = m_{Y'}$, $m_Z = m_{Z'}$, we have the following

constraints,

$$\begin{array}{lrcl} (M_Z^2 \;=) & (p_1+p_3+p_5+p_7)^2 & = & (p_2+p_4+p_6+p_8)^2, \\ (M_Y^2 \;=) & (p_1+p_3+p_5)^2 & = & (p_2+p_4+p_6)^2, \\ (M_X^2 \;=) & (p_1+p_3)^2 & = & (p_2+p_4)^2, \\ (M_N^2 \;=) & p_1^2 & = & p_2^2. \end{array} \tag{16}$$

where p_i is the 4-momentum for particle i $(i = 1 \ldots 8)$. Since the only invisible particles are 1 and 2 and since we can measure the missing transverse energy, there are two more constraints:

$$p_1^x + p_2^x = p_{miss}^x, \quad p_1^y + p_2^y = p_{miss}^y. \tag{17}$$

Given the 6 constraints in Eqs. (16) and (17) and 8 unknowns from the 4-momenta of the missing particles, there remain two unknowns per event. The system is under-constrained and cannot be solved. This situation changes if we use a second event with the same decay chains, under the assumption that the invariant masses are the same in the two events. Denoting the 4-momenta in the second event as q_i $(i = 1 \ldots 8)$, we have

8 more unknowns, q_1 and q_2, but 10 more equations,

$$\begin{aligned} q_1^2 &= q_2^2 &= p_2^2, \\ (q_1+q_3)^2 &= (q_2+q_4)^2 &= (p_2+p_4)^2, \\ (q_1+q_3+q_5)^2 &= (q_2+q_4+q_6)^2 &= (p_2+p_4+p_6)^2, \\ (q_1+q_3+q_5+q_7)^2 &= (q_2+q_4+q_6+q_8)^2 &= (p_2+p_4+p_6+p_8)^2, \end{aligned}$$

$$q_1^x + q_2^x = q_{miss}^x, \quad q_1^y + q_2^y = q_{miss}^y. \tag{18}$$

Altogether, we have 16 unknowns and 16 equations. The system can be solved numerically and we obtain discrete solutions for p_1, p_2, q_1, q_2 and thus the masses m_N, m_X, m_Y, and m_Z.

Note that the equations always have 8 complex solutions, but we will keep only the real and positive ones which we henceforth call "solutions".

Of course, the wrong solutions are different from pair to pair, but the correct solution is common.

It is easy to get lots of pairs of events.

We focus on the SPS1a decay chain $\widetilde{q} \to q\widetilde{\chi}_2^0 \to q\mu\widetilde{\mu}_R \to \widetilde{\chi}_1^0 q\mu\mu$ with SPS1a masses $m_{\widetilde{u},\widetilde{d}} = 564.8~\mathrm{GeV}, 570.8~\mathrm{GeV}$, $m_{\widetilde{\chi}_2^0} = 180.3~\mathrm{GeV}$, $m_{\widetilde{\mu}_R} = 142.5~\mathrm{GeV}$ and $m_{\widetilde{\chi}_1^0} = 97.4~\mathrm{GeV}$.

We first consider the ideal case: no background events, all visible momenta measured exactly, all intermediate particles on-shell and each visible particle associated with the correct decay chain and position in the decay chain.

We also restrict the squarks to be up-type only.

In this case, we can solve for the masses exactly by pairing any two events.

The only complication comes from there being 8 complex solutions for the system of equations, of which more than one can be real and positive.

The mass distributions for the ideal case with 100 events are shown in Fig. 15.

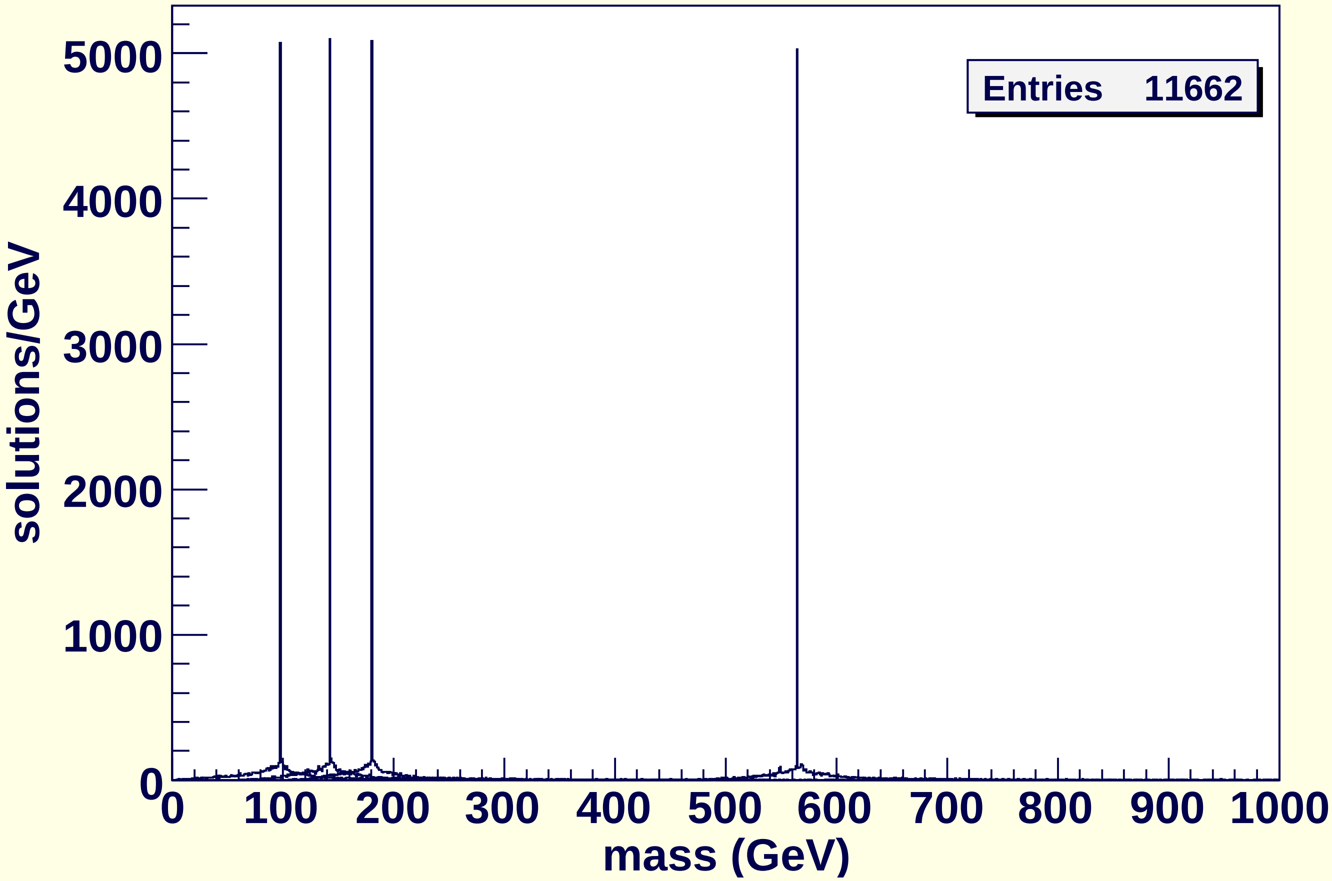

Figure 15: We plot the number of mass solutions (in 1 GeV bins — the same binning is used for the other plots) vs. mass in the ideal case. All possible pairs for 100 events are included.

As expected, we observe δ-function-like mass peaks on top of small backgrounds coming from wrong solutions. On average, there are about 2 solutions per pair of events.

The δ-functions in the mass distributions arise only when exactly correct momenta are input into the equations we solve.

To be experimentally realistic, we now include the following.

1. $\boxed{\text{Wrong combinations.}}$

For a given event a "combination" is a particular assignment of the jets and leptons to the external legs of Fig. 14. For each event, there is only one correct combination (excluding $1357 \leftrightarrow 2468$ symmetry).

Assuming that we can identify the two jets that correspond to the two quarks, we have 8 (16) possible combinations for the $2\mu 2e$ (4μ or $4e$) channel.

The total number of combinations for a pair of events is the product of the two, *i.e.* 64, 128 or 256.

Adding the wrong combination pairings for the ideal case yields the mass distributions of Fig. 16.

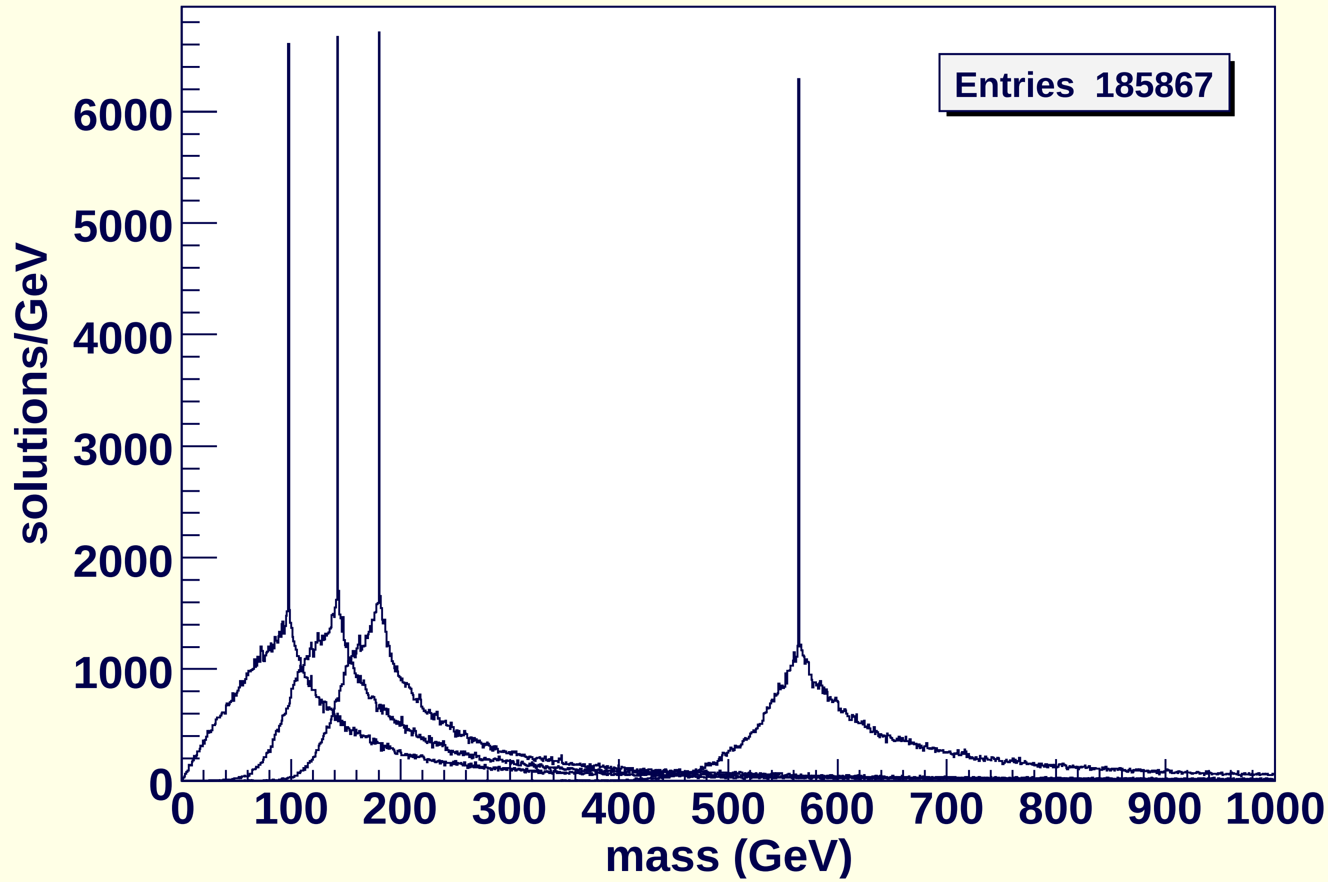

Figure 16: Number of mass solutions versus mass after including all combination pairings for 100 events.

Compared to Fig. 15, there are 16 times more (wrong) solutions, but the δ-function-like mass peaks remain evident.

2. $\boxed{\text{Finite widths.}}$ For SPS1a, the widths of the intermediate particles are roughly 5 GeV, 20 MeV and 200 MeV for $\widetilde{q}_L$, $\widetilde{\chi}_2^0$ and $\widetilde{\ell}_R$. Thus, the widths are quite small in comparison to the corresponding masses.

3. $\boxed{\text{Mass splitting between flavors.}}$ The masses for up and down type squarks have a small difference of 6 GeV. Since it is impossible to determine flavors for the light jets, the mass determined should be viewed as the average value of the two squarks (weighted by the parton distribution functions).

4. $\boxed{\text{Initial/final state radiation.}}$ These two types of radiation not only smear the visible particles' momenta, but also provide a source for extra jets in the events. We will apply a p_T cut to get rid of soft jets.

5. $\boxed{\text{Extra hard particles in the signal events.}}$ In SPS1a, many of the squarks come from gluino decay ($\widetilde{g} \to q\widetilde{q}_L$), which yields another hard q in the event. Fortunately, for SPS1a $m_{\widetilde{g}} - m_{\widetilde{q}_L} = 40~\mathrm{GeV}$ is much smaller than $m_{\widetilde{q}_L} - m_{\widetilde{\chi}_2^0} = 380~\mathrm{GeV}$. Therefore, the q from squark decay is usually much more energetic than the q from $\widetilde{g}$ decay. We select

the two jets with highest p_T in each event after cuts. Experimentally one would want to justify this choice by examining the jet multiplicity to ensure that this analysis is dominated by 2-jet events, and not 3 or 4 jet events. Furthermore, the softer jets will be an indication of clearly separable mass-differences.

6. $\boxed{\text{Background events.}}$ The SM backgrounds are negligible for this signal in SPS1a. There are a few significant backgrounds from other SUSY processes:

(a) $\widetilde{q}_L \to q\widetilde{\chi}_2^0 \to q\tau\widetilde{\tau} \to q\tau\tau\widetilde{\chi}_1^0$ for one or both decay chains, with all τ's decaying leptonically.

Indeed, $\widetilde{\chi}_2^0 \to \tau\widetilde{\tau}$ has the largest partial width, being 14 times that of $\widetilde{\chi}_2^0 \to \mu\tilde{\mu}$. However, to be included in our selection the two τ's in one decay chain must both decay to leptons with the same flavor, which reduces the ratio. A cut on lepton p_T also helps to reduce this background, since leptons from τ decays are softer.

Experimentally one should perform a separate search for hadronically decaying tau's or non-identical-flavor lepton decay chains to explicitly measure this background.

(b) Processes containing a pair of sbottoms, especially $\widetilde{b}_1$.

In SPS1a the first two generations of squarks are nearly degenerate. In any model, they must be discovered in a combined analysis since light quark jets are not distinguishable. Well-separated squark masses would show up as a double peak structure in M_Z. However b jets are distinguishable and a separate analysis should be performed to determine the b squark masses. This presents a background to the light squark search since b-tagging efficiency is only about 50% at high p_T.

(c) Processes that contain a pair of $\widetilde{\chi}_2^0$'s, not both coming from squark decays.

For these events to fake signal events, extra jets need to come from initial and/or final state radiation or other particle decays. For example, direct $\widetilde{\chi}_2^0$ pair production or $\widetilde{\chi}_2^0 + \widetilde{g}$ production. These are electroweak processes, but, since $\widetilde{\chi}_2^0$ has a much smaller mass than squarks, the cross-section is not negligible. In our SPS1a analysis, the large jet p_T cut reduces this kind of background due to the small $m_{\widetilde{g}} - m_{\widetilde{q}_L}$.

7. **Experimental resolutions.** In order to estimate this experimental effect at the LHC, we process all events with ATLFAST, a fast simulation

package of the ATLAS detector. Since we assume $300\ \mathrm{fb}^{-1}$ integrated luminosity, we run ATLFAST in the high luminosity mode.

The cuts used to isolate the signal are:

I) 4 isolated leptons with $p_T > 10$ GeV, $|\eta| < 2.5$ and matching flavors and charges consistent with our assumed $\widetilde{\chi}_2^0 \to \widetilde{\ell} \to \widetilde{\chi}_1^0$ decay;

II) No b-jets and ≥ 2 jets with $p_T > 100$ GeV, $|\eta| < 2.5$. The 2 highest-p_T jets are taken to be particles 7 and 8;

III) Missing $p_T > 50$ GeV.

For a data sample with $300\ \mathrm{fb}^{-1}$ integrated luminosity, there are about 1050 events left after the above cuts, out of which about 700 are signal events. After taking all possible pairs for all possible combinations and solving for the masses, we obtain the mass distributions in Fig. 17.

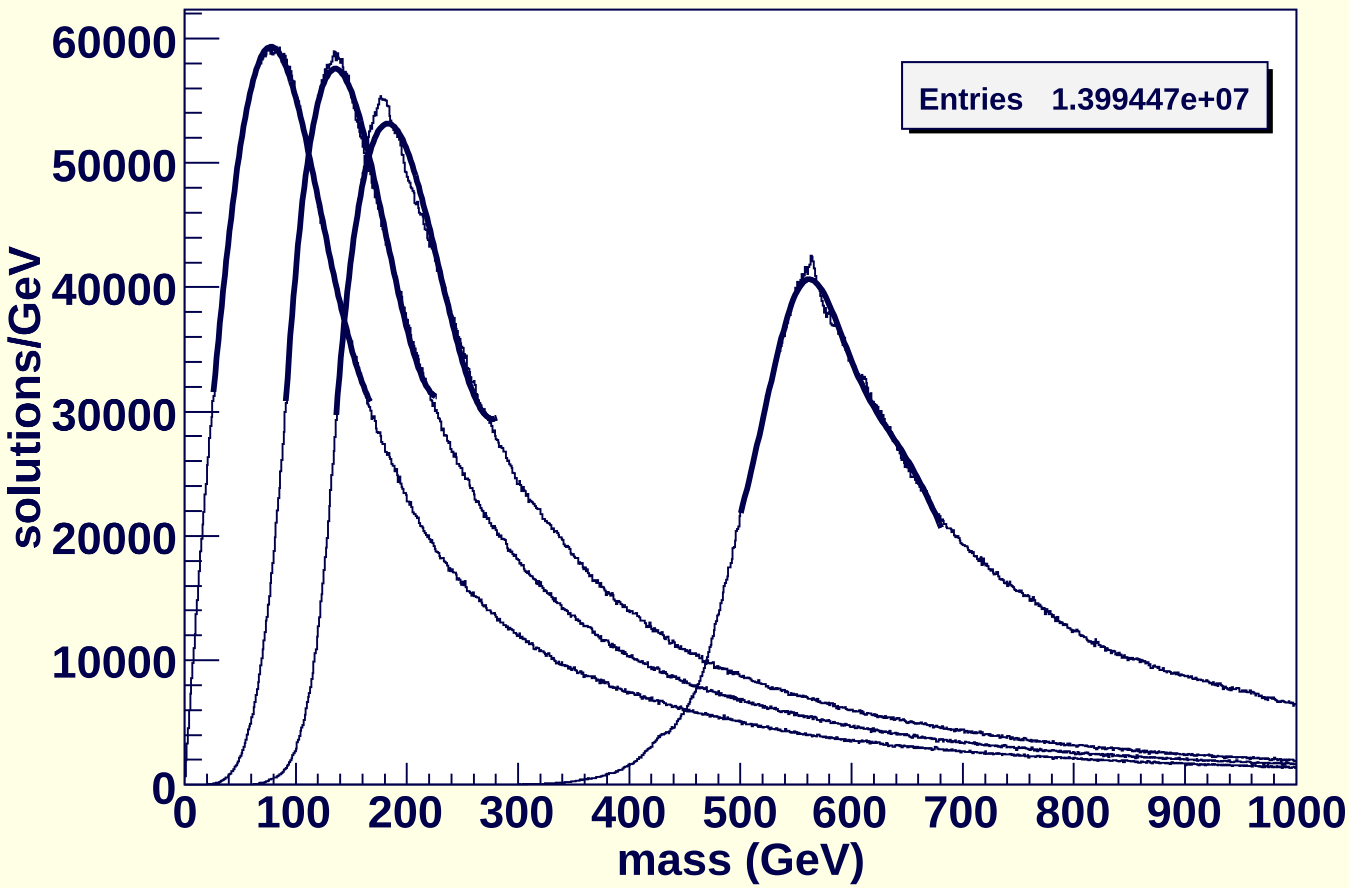

Figure 17: Mass solutions with all effects 1 – 7 included and after cuts I – III for the SPS1a SUSY model and $L = 300~\mathrm{fb}^{-1}$.

Fitting each distribution using a sum of a Gaussian plus a (single) quadratic polynomial and taking the maximum positions of the fitted peaks as the estimated masses yields $77.8, 135.6, 182.7, 562.0~\mathrm{GeV}$. Averaging over 10 different data samples, we find

$$m_N = 76.7 \pm 1.4 \text{ GeV}, \quad m_X = 135.4 \pm 1.5 \text{ GeV},$$
$$m_Y = 182.2 \pm 1.8 \text{ GeV}, \quad m_Z = 564.4 \pm 2.5 \text{ GeV}.$$

The statistical uncertainties are very small, but there exist biases, especially for the two light masses.

In practice, we can always correct the biases by comparing real data with Monte Carlo.

Nevertheless, it is perhaps more satisfying to reduce the biases as much as possible using data only.

In some cases, the biases can be very large and it is essential to reduce them before comparing with Monte Carlo.

The combinatorial background is an especially important source of bias since it yields peaked mass distributions that are not symmetrically distributed around the true masses, as can be seen from Fig. 16.

This will introduce biases that survive even after smearing. Therefore, we concentrate on reducing wrong solutions.

$\boxed{\text{First,}}$ we reduce the number of wrong combinations by the following procedure.

For each combination choice, c, for a given event, i ($i = 1, N_{evt}$), we count the number, $N_{pair}(c,i)$, of events that can pair with it (for some combination choice for the 2nd events) and give us solutions. We repeat this for every combination choice for every event.

Neglecting effects 2.– 7., $N_{pair}(c,i) = N_{evt} - 1$ if c is the correct combination for event i. After including backgrounds and smearing, $N_{pair}(c,i) < N_{evt} - 1$, but the correct combinations still have statistically larger $N_{pair}(c,i)$ than the wrong combinations.

Therefore, we cut on $N_{pair}(c,i)$. For the SPS1a model point, if $N_{pair}(c,i) \leq 0.75\, N_{evt}$ we discard the combination choice, c, for event i.

If all possible c choices for event i fail this criterion, then we discard event i altogether (implying a smaller N_{evt} for the next analysis cycle).

We then repeat the above procedure for the remaining events until no combinations can be removed.

After this, for the example data sample, the number of events is reduced

from 1050 (697 signal + 353 background) to 734 (539 signal + 195 background), and the average number of combinations per event changes from 11 to 4.

Second, **we increase the significance of the true solution by weighting events by $1/n$ where n is the number of solutions for the corresponding pair (using only the combination choices that have survived the previous cuts).**

This causes each pair (and therefore each event) to have equal weight in our histograms. Without this weighting, a pair with multiple solutions has more weight than a pair with a single solution, even though at most one solution would be correct for each pair.

Finally, **we exploit the fact that wrong solutions and backgrounds are much less likely to yield M_N, M_X, M_Y, and M_Z values that are all simultaneously close to their true values. We plot the $1/n$-weighted number of solutions as a function of the three mass differences (Fig. 18).**

We define mass difference windows by $0.6\times$ peak height and keep only those solutions for which *all three* **mass differences fall within the mass**

difference windows.

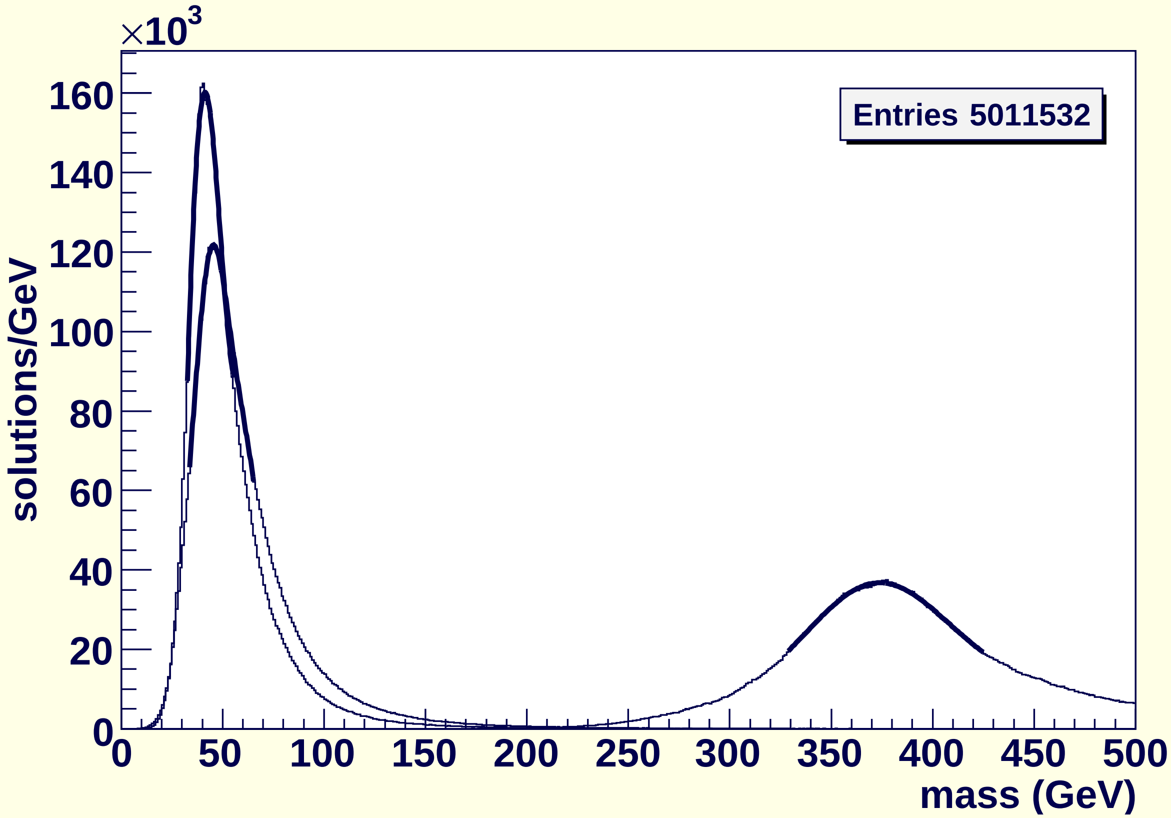

Figure 18: SPS1a, $L = 300$ fb^{-1} mass difference distributions.

The surviving solutions are plotted (without the $1/n$ weighting) in Fig. 19. Compared with Fig. 17, the mass peaks are narrower, more symmetric and the fitted values are less biased. The fitted masses are

$$m_N, m_X, m_Y, m_Z = 91.7, \quad 135.9, \quad 175.7 \quad 558.0 \text{ GeV}. \qquad (19)$$

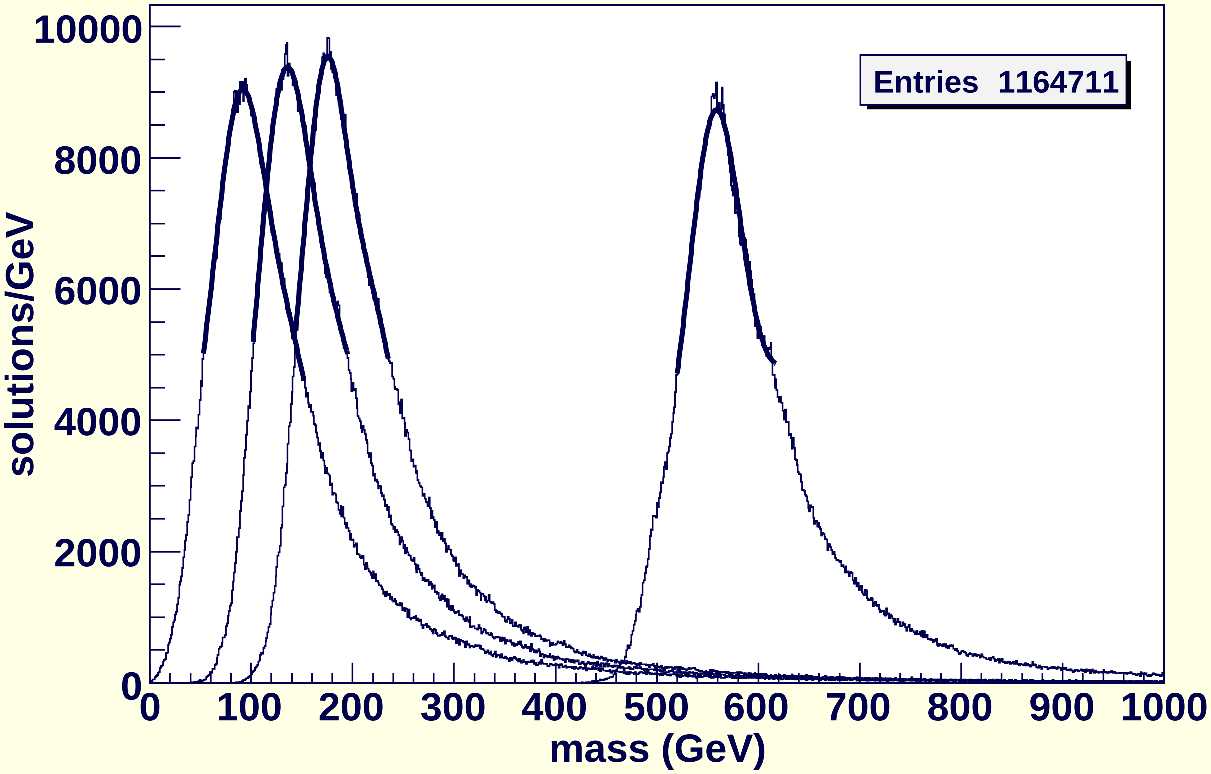

Figure 19: Final mass distributions after the bias-reduction procedure for the SPS1a SUSY model and $L = 300\ \mathrm{fb}^{-1}$.

Repeating the procedure for 10 data sets, we find

$$\begin{aligned} m_N &= 94.1 \pm 2.8 \text{ GeV}, \quad m_X = 138.8 \pm 2.8 \text{ GeV}, \\ m_Y &= 179.0 \pm 3.0 \text{ GeV}, \quad m_Z = 561.5 \pm 4.1 \text{ GeV}. \end{aligned}$$

vs. inputs of

$$\begin{aligned} m_N &= 97.4 \text{ GeV}, \quad m_X = 142.5, \\ m_Y &= 180.3 \text{ GeV}, \quad m_Z = 564.8, 570.8 \text{ GeV}. \end{aligned}$$

Thus, the biases are reduced at the cost of (slightly) increased statistical errors.

We reemphasize that the remaining biases in the above mass determinations can be removed by finding those input masses that yield the observed output masses (in fact mass distribution plots) after processing Monte Carlo generated data through our procedures. In this way, very accurate central mass values are obtained with the indicated statistical errors.

We have applied our method to other mass points to show its reliability.

We quote here results for "point 1" defined earlier with the following masses:

$$m_N, m_X, m_Y, m_Z = 85.3, 128.4, 246.6, 431.1/438.6 \text{ GeV}. \tag{20}$$

For 100 fb^{-1} of data, we have about 1220 events (1160 signal events) after the pre-bias-reduction cuts. After following a bias reduction procedure and using 10 data samples, we obtain

$$\begin{aligned} m_N &= 85 \pm 4 \text{ GeV}, \quad m_X = 131 \pm 4 \text{ GeV}, \\ m_Y &= 251 \pm 4 \text{ GeV}, \quad m_Z = 444 \pm 5 \text{ GeV}. \end{aligned}$$

Conclusions

- Using $\mathbf{2}$ chains with $\mathbf{2}$ visible particles each, $\Rightarrow \sim \boldsymbol{few}\ \mathrm{GeV}$ to $\mathbf{10}\ \mathrm{GeV}$ accuracy for the absolute mass scale is achievable at the LHC, depending upon the number of events available.

- Using $\mathbf{3}$ visible particles per chain improves further on this result to the point where it is slightly better than edge techniques.

  Consequences:

  1. The above accuracy, even in the difficult SPS1a case, should be sufficient to eliminate the 'slider' degeneracies of the LHC inverse solutions.
  2. The accuracy already achieved will aid enormously in the GUT extrapolation.
  3. It will also greatly increase the accuracy of the dark matter calculation.

- Our technique can, of course, be combined with the edge techniques (and others we had no time to discuss) to obtain the best possible overall mass scale and mass differences.

- **Don't forget that we must understand how to single out a single topology ($i.e.$ suppress others adequately) in the case that there are many new physics topologies.**

  If this cannot be done, then we must learn how to work with multiple topologies. We believe our techniques can be generalized to such a situation.